

however, was fairly high, and this does not necessarily relate to the clinical setting.

#### Downstream Signaling Pathway of the AT<sub>1</sub> Receptor Stimulation in the RVLM Involving ROS Production

As described above, activation of the AT<sub>1</sub> receptor produces superoxide anions as an initial step of ROS generation through NADPH oxidase. Thus, the signaling pathway should be pivotal for neuronal activation leading to hypertension via central sympathetic outflow. NAD(P)H oxidase-derived ROS production mediates the ANG II-induced pressor response via activation of p38 MAPK and ERK in the RVLM (18, 20). Chan et al. (20) demonstrated that intracerebroventricular infusion of ANG II elicits the long-term pressor response, and this pressor response is mediated by protein kinase C/ERK/cyclic adenosine monophosphate response element binding protein and *c-fos* induction (20). It should be noted that the ANG II-induced pressor response might not necessarily be related to ROS production in the RVLM. The ANG II-induced pressor response, however, is significantly inhibited by ROS scavenging, and endogenous blockade of AT<sub>1</sub> receptors in the brain stem of SHRSP reduces ROS and blood pressure (48, 91). Activation of caspase-3 acting through the Ras/p38 MAPK/ERK pathway in the RVLM might be involved in sympathoexcitation of SHRSP (65). In addition, the apoptotic proteins Bax and Bad are activated, and the antiapoptotic protein Bcl-2 is inhibited in the RVLM of SHRSP (65). The Ras inhibitor substantially attenuated these changes, thereby attenuating caspase-3 associated with the decrease in blood pressure. In contrast, however, c-Jun N-terminal kinase activity was not altered in the RVLM of SHRSP compared with that of WKY (65). It should be noted that the possibility of caspase-3-independent neuronal apoptosis in the RVLM or of a direct link between ROS and caspase-3 activation was not examined in that study (65). However, this finding is consistent with the results demonstrating that microinjection of ANG II induces AT<sub>1</sub> receptor-dependent ROS production and phosphorylation of p38 MAPK and ERK, but not stress-activated protein kinase/Jun N-terminal kinase in the RVLM of Sprague-Dawley rats (18). Interestingly, this is not the case in the RVLM of heart failure rabbits (77). Stress-activated protein kinase/Jun N-terminal kinase activity was increased in the RVLM of these heart failure rabbits (77). The increased phosphorylation of Jun N-terminal kinase may lead to activation of the transcription factor AP-1, which is a dimer of Jun and c-Fos family members. It is not clear why these differences between hypertension and heart failure occur. It is possible that signal transduction changes in the progression from hypertension to heart failure, thereby leading to further enhanced central sympathetic outflow. Further studies are needed to establish a more direct link between these signaling pathways, redox sensitivity, and the development and/or progression of hypertension.

#### Imbalance of Brain NO and ROS

Superoxide derived from NADPH oxidase reacts with and inactivates NO and thereby modulates its bioavailability (32, 97, 114) (Fig. 2). The converse is also true; that is, NO reduces superoxide, which may be beneficial (32, 99) (Fig. 2). An increase in NO in the RVLM decreases blood pressure and sympathetic nervous system activity to a greater extent in

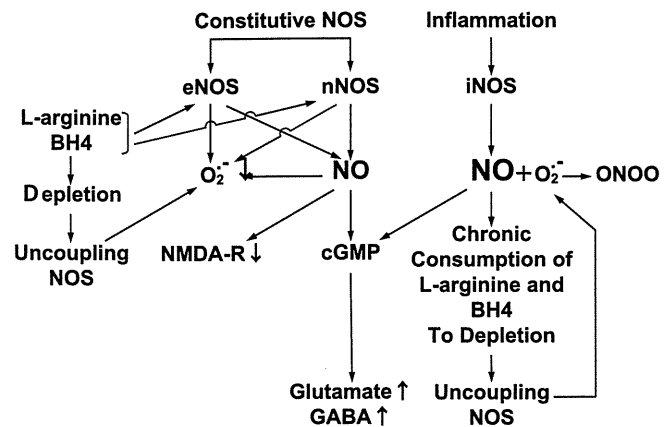


Fig. 2. A scheme demonstrating the interaction between nitric oxide (NO) and ROS generation. NMDA-R, *N*-methyl-D-aspartate receptors; GABA,  $\gamma$ -aminobutyric acid; BH4, tetrahydrobiopterin; NOS, nitric oxide synthase; eNOS, endothelial NOS; iNOS, inducible NOS; nNOS, neuronal NOS. [Modified from Hirooka (47).]

SHRSP than in WKY rats (58). This might be due to a reduction in superoxide via NO in the RVLM of SHRSP, which is increased in the RVLM of SHRSP (61). All three NOS isoforms generate superoxide depending on substrate (L-arginine) and cofactor (tetrahydrobiopterin) availability (32, 97, 114). The induction of both iNOS and ROS during inflammation is well established (88, 97). A recent study suggested that ROS and reactive nitrogen species, such as peroxynitrite dose-dependently regulate iNOS function (114). Overexpression of iNOS in the RVLM causes sympathoexcitation via an increase in oxidative stress (54). As expected, the release of more nitrite/nitrate ( $\text{NO}_x$ ) in RVLM dialysate is induced by iNOS overexpression than by eNOS overexpression (54). Relative to the constitutive isoforms, iNOS has approximately five-fold higher NO production (97).  $\text{NO}_x$  release, however, is increased by approximately twofold higher by iNOS overexpression than by eNOS overexpression (54). We considered that the precursor of NO production, L-arginine, and its cofactor, tetrahydrobiopterin, might be consumed and insufficient when iNOS is chronically expressed, thereby iNOS would produce superoxide instead of NO (Fig. 2). Otherwise, chronic overexpression of iNOS increases levels of NO chronically, which, in turn, reacts with superoxide in a diffusion-limited reaction to produce peroxynitrite (Fig. 2). In fact, we found an increase in the TBARS levels in the RVLM and the pressor response after overexpression of iNOS. The increased pressor response was, however, abolished by iNOS inhibitors or Tempol. Once ROS production is increased, ROS enhance superoxide production from iNOS, indicating that ROS promote iNOS uncoupling. Further, peroxynitrite, produced from the reaction between NO and superoxide, reduces both NO and superoxide generation, indicating that peroxynitrite causes iNOS dysfunction enzymatically. In our study, we detected some iNOS-positive cells with the antinitrotyrosine antibody (54). Furthermore, iNOS expression levels were increased in the RVLM of SHRSP compared with WKY (56). Kung et al. (68) suggested that mitochondrial respiratory enzyme complexes in the RVLM were cellular targets of NO and ROS interaction after eNOS gene transfer. This concept is problematic, however, in that they suggest that superoxide and per-

oxynitrite are produced after eNOS gene transfer into the RVLM (68). Another recent study suggested that NMDA receptor activation increases ROS production through NO and Nox2 (33). Further studies are needed to explore whether this mechanism functions via ubiquitous glutamatergic synaptic transmission in vivo.

#### *Sympathoinhibitory Effects of Antihypertensive Drugs and Statins*

NADPH oxidase, which is activated by AT<sub>1</sub> receptor stimulation, is a major source of ROS (11, 17, 113, 135). The specific brain nuclei that regulate SNA, such as the anteroventral third ventricle, paraventricular nucleus of the hypothalamus, NTS, and the RVLM, are rich in AT<sub>1</sub> receptors (2, 10, 26, 28, 83). AT<sub>1</sub> receptor expression levels are upregulated in the RVLM of hypertensive animal models compared with normotensive controls (105). Thus, it is possible that AT<sub>1</sub> receptor blockers reduce oxidative stress in the brain, as well as in the peripheral vasculature. It is also possible that AT<sub>1</sub> receptor blockers inhibit ROS production by blocking AT<sub>1</sub> receptor-mediated intracellular signaling (11, 48, 50) and that this antioxidant action accounts for the absence of reflex-induced sympathoexcitation after treatment with AT<sub>1</sub> receptor blockers. We evaluated the effects of AT<sub>1</sub> receptor blockers, olmesartan and telmisartan, on brain oxidative stress in SHRSP (4, 48). Both AT<sub>1</sub> receptor blockers have antioxidant properties in the brain without stimulating reflex-mediated SNA in SHRSP. We used in vivo ESR spectroscopy to examine the effect of oral olmesartan on oxidative stress in the brain (4), because the in vivo ESR method is a powerful technique for evaluating oxidative stress (3, 110, 111). The effects of peripherally administered olmesartan or telmisartan on central sympathetic outflow have been demonstrated in other studies (34, 76). Are these antioxidant effects of olmesartan or telmisartan specific for each drug or the AT<sub>1</sub> receptor blocker class? Other angiotensin receptor blockers, such as losartan or candesartan, have similar sympatho-inhibitory effects in the CNS, although there are some differences among angiotensin receptor blockers (24, 89, 102, 124). The differences of the central effects of each angiotensin receptor blocker might depend on its lipophilicity, pharmacokinetics, and the transporter system (24, 34, 48, 124). Furthermore, systemically administered candesartan reduces brain ANG II via downregulation of the brain renin-angiotensin system (98). This finding provides new mechanistic insight into the treatment of hypertension by the AT<sub>1</sub> receptor blockers (84). Unfortunately, however, these effects of AT<sub>1</sub> receptor blockers, that is, reduction of brain oxidative stress and sympatho-inhibitory effects, even when administered systemically, are usually ignored by researchers or clinicians, but should be considered as potential therapeutic candidates.

Considering the inhibitory effects of AT<sub>1</sub> receptor blockers on brain oxidative stress and sympathetic nervous system activity, it would be interesting to know whether other cardiovascular drugs have similar effects. We found that atorvastatin causes depressor and sympathoinhibitory effects with upregulation of NOS in SHRSP (59), which is consistent with the effects of statins on eNOS upregulation in the vasculature (55). Atorvastatin also reduces oxidative stress in the RVLM of SHRSP (62, 63, 64). With regard to the central sympathoinhibitory effects of calcium channel blockers, lipophilic dihy-

dropyridine calcium channel blockers, such as nifedipine, nisoldipine, and amlodipine, readily cross the blood-brain barrier, thereby presumably blocking brain L-type Ca<sup>2+</sup> channels leading to central sympathoinhibition (73). It is generally considered that an arterial baroreflex-mediated increase in sympathetic activity is responsible for the unfavorable effects of short- and strong-acting dihydropyridine calcium channel blockers; therefore, the intrinsic sympathoinhibitory effects of calcium channel blockers have been ignored. These findings together suggest that increased NOS activity and antioxidant effects in the brain stem might be involved in the central sympathoinhibitory effects of some calcium channel blockers (45, 55, 67). The precise mechanisms involved, however, remain unknown, and further studies are required.

#### *Summary and Conclusions*

In summary, accumulating evidence indicates that an imbalance of NO and ROS in the CNS, particularly in the brain stem, is crucially involved in hypertension via the activation of central sympathetic outflow. Upstream and downstream consequences of the precise mechanisms are discussed. Several questions remain, however, because the interactions between NO and ROS are complex. Further studies are required to gain a better understanding of the role of brain NO and ROS in autonomic cardiovascular regulation and potential therapeutic targets.

#### GRANTS

This series of studies was supported by the Grants-in Aid for Scientific Research from the Japan Society for Promotion of Science and, in part, by a Grant from Kimura Memorial Foundation Research.

#### DISCLOSURES

No conflicts of interest, financial or otherwise, are declared by the authors.

#### REFERENCES

1. Alaghand-Zadeh J, Das I, Hanson MR, MacGregor CAL, de Wardener HE, Laycock JF. Hypothalamic and plasma total nitrate/nitrite concentrations in spontaneously hypertensive rats. *Exp Physiol* 81: 881–883, 1996.
2. Allen AM, O'Callaghan EL, Chen D, Bassi JK. Central neural regulation of cardiovascular function by angiotensin: a focus on the rostral ventrolateral medulla. *Neuroendocrinology* 89: 361–369, 2009.
3. Anzai K, Saito K, Takeshita K, Takahashi S, Miyazaki H, Shoji H, Lee MC, Masumizu T, Ozawa T. Assessment of ESR-CT imaging by comparison with autoradiography for the distribution of a blood-brain-barrier permeable spin probe, MC-PROXYL, to rodent brain. *Magn Reson Imaging* 21: 765–772, 2003.
4. Araki S, Hirooka Y, Kishi T, Yasukawa K, Utsumi H, Sunagawa K. Olmesartan reduces oxidative stress in the brain of stroke-prone spontaneously hypertensive rats assessed by an in vivo ESR method. *Hypertens Res* 32: 1091–1096, 2009.
5. Bai Y, Jabbari B, Ye S, Campese VM. Regional expression of NAD(P)H oxidase and superoxide dismutase in the brain of rats with neurogenic hypertension. *Am J Nephrol* 29: 483–492, 2009.
6. Bains JS, Ferguson AV. Nitric oxide depolarizes type II paraventricular nucleus neurons in vitro. *Neuroscience* 79: 149–159, 1997.
7. Bains JS, Ferguson AV. Nitric oxide regulates NMDA-driven GABAergic inputs to type I neurons of the rat paraventricular nucleus. *J Physiol* 499: 733–746, 1997.
8. Batten TFC, Atkinson L, Deuchars J. Nitric oxide systems in the medulla oblongata and their involvement in autonomic control. In: *Functional Neuroanatomy of the Nitric Oxide System. Handbook of Chemical Neuroanatomy*, edited by Steinbusch HWM, De Vente J, Vincent SR, Amsterdam, The Netherlands: Elsevier, 177–213, 2000.

9. **Bergamaschi CT, Campos RR, Lopes OU.** Rostral ventrolateral medulla: a source of sympathetic activation in rats subjected to long-term treatment with L-NAME. *Hypertension* 34: 744–747, 1999.
10. **Bourassa EA, Sved AF, Speth RC.** Angiotensin modulation of rostral ventrolateral medulla (RVLM) in cardiovascular regulation. *Mol Cell Endocrinol* 302: 167–175, 2009.
11. **Brandes RP.** Vascular functions of NADPH oxidases. *Hypertension* 56: 17–21, 2010.
12. **Briones AM, Touyz RM.** Oxidative stress and hypertension: current concepts. *Curr Hypertens Rep* 12: 135–142, 2010.
13. **Cabrena CL, Bealer SL, Bohr DF.** Central depressor action of nitric oxide is deficient in genetic hypertension. *Am J Hypertens* 9: 237–241, 1996.
14. **Campese VM, Sindhu RK, Ye S, Bai Y, Vaziri ND, Jabbari B.** Regional expression of NO synthase, NAD(P)H oxidase and superoxide dismutase in the rat brain. *Brain Res* 1134: 27–32, 2007.
15. **Campese VM, Shaohua Y, Huiquin Z.** Oxidative stress mediates angiotensin II-dependent stimulation of sympathetic nerve activity. *Hypertension* 46: 533–539, 2005.
16. **Campos RR, Bergamaschi CT.** Neurotransmission alterations in central cardiovascular control in experimental hypertension. *Curr Hypertens Rev* 2: 193–198, 2006.
17. **Campos RR.** Oxidative stress in the brain and arterial hypertension. *Hypertens Res* 32: 1047–1048, 2009.
18. **Chan SHH, Hsu KS, Huang CC, Wang LL, Ou CC, Chan JYH.** NADPH oxidase-derived superoxide anion mediates angiotensin II-induced pressor effect via activation of p38 mitogen-activated protein kinase in the rostral ventrolateral medulla. *Circ Res* 97: 772–780, 2005.
19. **Chan SHH, Tai MH, Li CY, Chan JYH.** Reduction in molecular synthesis or enzyme activity of superoxide dismutase and catalase contributes to oxidative stress and neurogenic hypertension in spontaneously hypertensive rats. *Free Radic Biol Med* 40: 2028–2039, 2006.
20. **Chan SHH, Wang LL, Tseng HL, Chan JYH.** Upregulation of AT<sub>1</sub> receptor gene on activation of protein kinase C $\beta$ /nicotinamide adenine dinucleotide diphosphate oxidase/ERK1/2/c-fos signaling cascade mediates long-term pressor effect of angiotensin II in rostral ventrolateral medulla. *J Hypertens* 25: 1845–1861, 2007.
21. **Chan SHH, Wu KLH, Chang AYW, Tai MH, Chan JYH.** Oxidative impairment of mitochondrial electron transport chain complexes in rostral ventrolateral medulla contributes to neurogenic hypertension. *Hypertension* 53: 217–227, 2009.
22. **Chan SHH, Wu CA, Wu KLH, Ho YH, Chang AYW, Chan JYH.** Transcriptional upregulation of mitochondrial uncoupling protein 2 protects against oxidative stress-associated neurogenic hypertension. *Circ Res* 105: 886–896, 2009.
23. **Chan SHH, Wu KLH, Kung PSS, Chan JYH.** Oral intake of rosiglitazone promotes a central antihypertensive effect via upregulation of peroxisome proliferator-activated receptor- and alleviation of oxidative stress in rostral ventrolateral medulla of spontaneously hypertensive rats. *Hypertension* 55: 1444–1453, 2010.
24. **Culman J, Blume A, Gohlke P, Unger T.** The renin-angiotensin system in the brain: possible therapeutic implications for AT<sub>1</sub>-receptor blockers. *J Hum Hypertens* 16: S64–S70, 2002.
25. **Dampney RAL.** Functional organization of central pathways regulating the cardiovascular system. *Physiol Rev* 74: 323–364, 1994.
26. **Dampney RAL, Fontes MAP, Hirooka Y, Potts PD, Tagawa T.** Role of angiotensin II receptors in the regulation of vasomotor neurons in the rostral ventrolateral medulla. *Clin Exp Pharmacol Physiol* 29: 467–472, 2002.
27. **Dias AC, Vitela M, Colombari E, Mifflin SW.** Nitric oxide modulation of glutamatergic, baroreflex, and cardiopulmonary transmission in the nucleus of the solitary tract. *Am J Physiol Heart Circ Physiol* 288: H256–H262, 2005.
28. **Dupont AG, Brouwers S.** Brain angiotensin peptides regulate sympathetic tone and blood pressure. *J Hypertens* 28: 1599–1610, 2010.
29. **Eshima K, Hirooka Y, Shigematsu H, Matsuo I, Koike G, Sakai K, Takeshita A.** Angiotensin in the nucleus tractus solitarius contributes to neurogenic hypertension caused by chronic nitric oxide synthase inhibition. *Hypertension* 36: 259–263, 2000.
30. **Esler M.** Sympathetic nervous activation in essential hypertension: commonly neglected as a therapeutic target, usually ignored as a drug side effect. *Hypertension* 55: 1090–1091, 2010.
31. **Esler M.** The 2009 Carl Ludwig Lecture. Pathophysiology of the human sympathetic nervous system in cardiovascular diseases: the translation from mechanisms to medical management. *J Appl Physiol* 108: 227–237, 2010.
32. **Garthwaite J.** Concepts of neural nitric oxide-mediated transmission. *Eur J Neurosci* 27: 2783–2802, 2008.
33. **Girouard H, Wang G, Gallo EF, Anthrather J, Zhou P, Pickel VM, Iadecola C.** NMDA receptor activation increases free radical production through nitric oxide and Nox2. *J Neurosci* 29: 2545–2552, 2009.
34. **Gohlke P, Weiss S, Jansen A, Wienen W, Stangier J, Rascher W, Culman J, Unger T.** AT<sub>1</sub> receptor antagonist telmisartan administered peripherally inhibits central responses to angiotensin II in conscious rats. *J Pharmacol Exp Ther* 298: 62–70, 2001.
35. **Grassi G.** Assessment of sympathetic cardiovascular drive in human hypertension: achievements and perspectives. *Hypertension* 54: 690–697, 2009.
36. **Grassi G.** Sympathetic neural activity in hypertension and related diseases. *Am J Hypertens* 23: 1052–1060, 2010.
37. **Grassi G, Seravalle G, Quarti-Trevano F.** The ‘neurogenic hypothesis’ in hypertension: current evidence. *Exp Physiol* 95: 581–586, 2010.
38. **Guyenet PG.** The sympathetic control of blood pressure. *Nat Rev Neurosci* 7: 335–346, 2006.
39. **Harada S, Tokunaga S, Momohara M, Masaki H, Tagawa T, Imai-zumi T, Takeshita A.** Inhibition of nitric oxide formation in the nucleus tractus solitarius increases renal sympathetic nerve activity in rabbits. *Circ Res* 72: 511–516, 1993.
40. **Häfner W, Sassmann A, Qadri F, Jöhren O, Dominiak P.** Expression of nitric oxide synthase isoforms in hypothalamo-pituitary-adrenal axis during the development of spontaneously hypertension in rats. *Mol Brain Res* 138: 198–204, 2005.
41. **Hironaga K, Hirooka Y, Matsuo I, Shihara M, Tagawa T, Harasawa Y, Takeshita A.** Role of endogenous nitric oxide in the brain stem on the rapid adaptation of baroreflex. *Hypertension* 31: 27–31, 1998.
42. **Hirooka Y, Polson JW, Dampney RAL.** Pressor and sympathoexcitatory effects of nitric oxide in the rostral ventrolateral medulla. *J Hypertens* 14: 1317–1324, 1996.
43. **Hirooka Y, Kishi T, Sakai K, Shimokawa H, Takeshita A.** Effect of overproduction of nitric oxide in the brain stem on the cardiovascular response in conscious rats. *J Cardiovasc Pharmacol* 41 Suppl 1: S119–S126, 2003.
44. **Hirooka Y, Sakai K, Kishi T, Ito K, Shimokawa H, Takeshita A.** Enhanced depressor response to endothelial nitric oxide synthase gene transfer into the nucleus tractus solitarius of spontaneously hypertensive rats. *Hypertens Res* 26: 325–331, 2003.
45. **Hirooka Y, Kimura Y, Nozoe M, Sagara Y, Ito K, Sunagawa K.** Amlodipine-induced reduction of oxidative stress in the brain is associated with sympatho-inhibitory effects in stroke-prone spontaneously hypertensive rats. *Hypertens Res* 29: 49–56, 2006.
46. **Hirooka Y.** Localized gene transfer and its application for the study of central cardiovascular control. *Auton Neurosci* 126–127: 120–129, 2006.
47. **Hirooka Y.** Role of reactive oxygen species in brainstem in neural mechanisms of hypertension. *Auton Neurosci* 142: 20–24, 2008.
48. **Hirooka Y, Sagara Y, Kishi T, Sunagawa K.** Oxidative stress and central cardiovascular regulation: pathogenesis of hypertension and therapeutic aspects. *Circ J* 74: 827–835, 2010.
49. **Horn T, Smith PM, McLaughlin BE, Bauce L, Marks GS, Pittman QJ, Ferguson AV.** Nitric oxide actions in paraventricular nucleus: cardiovascular and neurochemical implications. *Am J Physiol Regul Integr Comp Physiol* 266: R306–R313, 1994.
50. **Inaba S, Iwai M, Furuno M, Tomono Y, Senba I, Okayama H, Mogi M, Higaki J, Horiuchi M.** Continuous activation of renin-angiotensin system impairs cognitive function in renin/angiotensinogen transgenic mice. *Hypertension* 53: 356–362, 2009.
51. **Infanger DW, Shrama RV, Davisson RL.** NADPH oxidases of the brain: distribution, regulation, and function. *Antioxid Redox Signal* 8: 1583–1596, 2006.
52. **Judy WV, Watanabe AM, Henry DP, Besch HR, Murphy WR, Hockel GM.** Sympathetic nerve activity: role in regulation of blood pressure in the spontaneously hypertensive rat. *Circ Res* 38: I-121–I-129, 1976.
53. **Kagiyama S, Tsuchihashi T, Abe I, Fujishima M.** Cardiovascular effects of nitric oxide in the rostral ventrolateral medulla of rats. *Brain Res* 757: 155–158, 1997.
54. **Kimura Y, Hirooka Y, Sagara Y, Ito K, Kishi T, Shimokawa H, Takeshita A, Sunagawa K.** Overexpression of inducible nitric oxide synthase in rostral ventrolateral medulla causes hypertension and sym-

- pathoexcitation via an increase in oxidative stress. *Circ Res* 96: 252–260, 2005.
55. **Kimura Y, Hirooka Y, Sagara Y, Sunagawa K.** Long-acting calcium channel blocker, azelnidipine, increases endothelial nitric oxide synthase in the brain and inhibits sympathetic nerve activity. *Clin Exp Hypertens* 29: 13–21, 2007.
  56. **Kimura Y, Hirooka Y, Kishi T, Ito K, Sagara Y, Sunagawa K.** Role of inducible nitric oxide synthase in rostral ventrolateral medulla in blood pressure regulation in spontaneously hypertensive rats. *Clin Exp Hypertens* 31: 281–286, 2009.
  57. **Kishi T, Hirooka Y, Shigematsu H, Shimokawa H, Takeshita A.** Overexpression of eNOS in the RVLM causes hypotension and bradycardia via GABA release. *Hypertension* 38: 896–901, 2001.
  58. **Kishi T, Hirooka Y, Ito K, Sakai K, Shimokawa H, Takeshita A.** Cardiovascular effects of overexpression of endothelial nitric oxide synthase in the rostral ventrolateral medulla in stroke-prone spontaneously hypertensive rats. *Hypertension* 39: 264–268, 2002.
  59. **Kishi T, Hirooka Y, Mukai Y, Shimokawa H, Takeshita A.** Atorvastatin causes depressor and sympatho-inhibitory effect with upregulation of nitric oxide synthases in stroke-prone hypertensive rats. *J Hypertens* 21: 379–386, 2003.
  60. **Kishi T, Hirooka Y, Kimura Y, Sakai K, Ito K, Shimokawa H, Takeshita A.** Overexpression of eNOS in RVLM improves impaired baroreflex control of heart rate in SHRSP. *Hypertension* 41: 255–260, 2003.
  61. **Kishi T, Hirooka Y, Kimura Y, Ito K, Shimokawa H, Takeshita A.** Increased reactive oxygen species in rostral ventrolateral medulla contribute to neural mechanisms of hypertension in stroke-prone spontaneously hypertensive rats. *Circulation* 109: 2357–2362, 2004.
  62. **Kishi T, Hirooka Y, Shimokawa H, Takeshita A, Sunagawa K.** Atorvastatin reduces oxidative stress in the rostral ventrolateral medulla of stroke-prone spontaneously hypertensive rats. *Clin Exp Hypertens* 30: 3–11, 2008.
  63. **Kishi T, Hirooka Y, Konno S, Sunagawa K.** Atorvastatin improves the impaired baroreflex sensitivity via anti-oxidant effect in the rostral ventrolateral medulla of SHRSP. *Clin Exp Hypertens* 31: 698–704, 2009.
  64. **Kishi T, Hirooka Y, Konno S, Sunagawa K.** Sympathoinhibition induced by centrally administered atorvastatin is associated with alteration of NAD(P)H and Mn-SOD activity in rostral ventrolateral medulla of stroke-prone SHR. *J Cardiovasc Pharmacol* 55: 184–190, 2010.
  65. **Kishi T, Hirooka Y, Konno S, Ogawa K, Sunagawa K.** Angiotensin type 1 receptor-activated caspase-3 through ras/mitogen-activated protein kinase/extracellular signal-regulated kinase in the rostral ventrolateral medulla is involved in sympathoexcitation in stroke-prone spontaneously hypertensive rats. *Hypertension* 55: 291–297, 2010.
  66. **Koga Y, Hirooka Y, Araki S, Nozoe M, Kishi T, Sunagawa K.** High salt intake enhances blood pressure increase during development of hypertension via oxidative stress in rostral ventrolateral medulla of spontaneously hypertensive rats. *Hypertens Res* 31: 2075–2083, 2008.
  67. **Konno S, Hirooka Y, Araki S, Koga Y, Kishi T, Sunagawa K.** Azelnidipine decreases sympathetic nerve activity via antioxidant effect in the rostral ventrolateral medulla of stroke-prone spontaneously hypertensive rats. *J Cardiovasc Pharmacol* 52: 555–560, 2008.
  68. **Kung LC, Chan SHH, Wu KLH, Ou CC, Tai MH, Chan JYH.** Mitochondrial respiratory enzyme complexes in rostral ventrolateral medulla as cellular targets of nitric oxide and superoxide interaction in the antagonism of antihypertensive action of eNOS transgene. *Mol Pharmacol* 74: 1319–1332, 2008.
  69. **Kurukoff TL, Gehlen F, Ganten D, Wagner J.** Gene expression of brain nitric oxide synthase and soluble guanylate cyclase in hypothalamus and medulla of two-kidney, one-clip hypertensive rats. *Hypertension* 26: 171–176, 1995.
  70. **Krukoff TL.** Central action of nitric oxide in regulation of autonomic functions. *Brain Res Rev* 30: 52–65, 1999.
  71. **Lambeth JD.** Nox enzymes, ROS, and chronic disease: an example of antagonistic pleiotropy. *Free Radic Biol Med* 43: 332–347, 2007.
  72. **Lassegue B, Clempus RE.** Vascular NAD(P)H oxidases: specific features, expression, and regulation. *Am J Physiol Regul Integr Comp Physiol* 285: R277–R297, 2003.
  73. **Leenen FHH, Ruzicka M, Huang BS.** Central sympathoinhibitory effects of calcium channel blockers. *Curr Hypertens Res* 3: 314–321, 2001.
  74. **Lin HC, Kang BH, Wan FJ, Huang ST, Tseng CJ.** Reciprocal regulation of nitric oxide and glutamate in the nucleus tractus solitarii of rats. *Eur J Pharmacol* 407: 83–89, 2000.
  75. **Lin LH.** Glutamatergic neurons say NO in the nucleus tractus solitarii. *J Chem Neuroanat* 38: 1154–1165, 2009.
  76. **Lin Y, Matsumura K, Kagiya S, Fukuhara M, Fujii K, Iida M.** Chronic administration of olmesartan attenuates the exaggerated pressor response to glutamate in the rostral ventrolateral medulla of SHR. *Brain Res* 1058: 161–166, 2005.
  77. **Liu D, Gao L, Roy SK, Cornish KG, Zucker IH.** Neuronal angiotensin II type 1 receptor upregulation in heart failure: activation of activator protein 1 and jun N-terminal kinase. *Circ Res* 99: 1004–1011, 2006.
  78. **Liu JL, Murakami H, Zucker IH.** Effects of NO on baroreflex control of heart rate and renal nerve activity in conscious rabbits. *Am J Physiol Regul Integr Comp Physiol* 270: R1361–R1370, 1996.
  79. **Luft FC, Demmert G, Rohmeiss P, Unger T.** Baroreceptor reflex effect on sympathetic nerve activity in stroke-prone spontaneously hypertensive rats. *J Auton Nerv Syst* 17: 199–209, 1986.
  80. **Ma S, Abboud FM, Felder RB.** Effects of L-arginine-derived nitric oxide synthesis on neuronal activity in nucleus tractus solitarius. *Am J Physiol Regul Integr Comp Physiol* 268: R487–R491, 1995.
  81. **Marting-Pinge MC, Baraldi-Passy I, Lopes OU.** Excitatory effects of nitric oxide within the rostral ventrolateral medulla of freely moving rats. *Hypertension* 30: 704–707, 1997.
  82. **Matsuo I, Hirooka Y, Hironaga K, Eshima K, Shigematsu H, Shihara M, Sakai K, Takeshita A.** Glutamate release via NO production evoked by NMDA in the NTS enhances hypotension and bradycardia in vivo. *Am J Physiol Regul Integr Comp Physiol* 280: R1285–R1291, 2001.
  83. **McKinley MJ, Albinson AL, Allen AM, Mathai M, May CN, McAllen RM, Oldfield BJ, Mendelsohn FAO, Chai SY.** The brain renin-angiotensin system: location and physiological roles. *Int J Biochem Cell Biol* 35: 901–918, 2003.
  84. **Mogi M, Horiuchi M.** Remote control of brain angiotensin II levels by angiotensin receptor blockers. *Hypertens Res* 33: 116–117, 2010.
  85. **Morimoto S, Cassel MD, Beltz TG, Johnson AK, Davison RL, Sigmund CD.** Elevated blood pressure in transgenic mice with brain-specific expression of human angiotensinogen driven by the glial fibrillary acidic protein promoter. *Circ Res* 89: 365–372, 2001.
  86. **Morimoto S, Cassel MD, Sigmund CD.** The brain renin-angiotensin system in transgenic mice carrying a highly regulated human renin transgene. *Circ Res* 90: 80–86, 2002.
  87. **Murakami H, Liu JL, Yoneyama H, Nishida Y, Okada K, Kosaka H, Morita H, Zucker IH.** Blockade of neuronal nitric oxide synthase alters the baroreflex control of heart rate in the rabbit. *Am J Physiol Regul Integr Comp Physiol* 274: R181–R186, 1998.
  88. **Murphy S, Gibson CL.** Nitric oxide, ischaemia and brain inflammation. *Biochem Soc Trans* 35: 1133–1137, 2007.
  89. **Nishimura Y, Ito T, Hoe KL, Saavedra JM.** Chronic peripheral administration of the angiotensin II AT<sub>1</sub> receptor antagonist candesartan blocks brain AT<sub>1</sub> receptors. *Brain Res* 871: 29–38, 2000.
  90. **Nozoe M, Hirooka Y, Koga Y, Sagara Y, Kishi T, Engelhardt JF, Sunagawa K.** Inhibition of racl-derived reactive oxygen species in nucleus tractus solitarius decreases blood pressure and heart rate in stroke-prone spontaneously hypertensive rats. *Hypertension* 50: 62–68, 2007.
  91. **Nozoe M, Hirooka Y, Koga Y, Araki S, Konno S, Kishi T, Ide T, Sunagawa K.** Mitochondria-derived reactive oxygen species mediate sympathoexcitation induced by angiotensin II in the rostral ventrolateral medulla. *J Hypertens* 26: 2176–2184, 2008.
  92. **Oliveira-Sales EB, Dugaich AP, Carillo BA, Abreu NP, Boim MA, Martins PJ, D'Almeida V, Dolnikoff MS, Bergamaschi CT, Campos RR.** Oxidative stress contributes to renovascular hypertension. *Am J Hypertens* 21: 98–104, 2008.
  93. **Oliveira-Sales EB, Nishi EE, Carillo BA, Dolnikoff MS, Bergamaschi CT, Campos RR.** Oxidative stress in the sympathetic premotor neurons contributes to sympathetic activation in renovascular hypertension. *Am J Hypertens* 22: 484–492, 2009.
  94. **Paravicini T, Touyz RM.** Redox signaling in hypertension. *Cardiovasc Res* 71: 247–258, 2006.
  95. **Patel KP, Li YF, Hirooka Y.** Role of nitric oxide in central sympathetic outflow. *Exp Biol Med (Maywood)* 226: 814–824, 2001.

96. Paton JFR, Waki H, Abdala APL, Dickinson J, Kasparov S. Vascular-brain signaling in hypertension: role of angiotensin II and nitric oxide. *Curr Hypertens Rep* 9: 242–247, 2007.
97. Pannu R, Singh I. Pharmacological strategies for the regulation of inducible nitric oxide synthase: neurogenerative versus neuroprotective mechanisms. *Neurochem Intl* 49: 170–182, 2006.
98. Pelisch N, Hosomi N, Ueno M, Masugata H, Murao K, Hitomi H, Nakao D, Kobori H, Nishiyama A, Kohno M. Systemic candesartan reduces brain angiotensin II via downregulation of brain renin-angiotensin system. *Hypertens Res* 33: 161–164, 2010.
99. Peterson JR, Shrama RV, Davisson RL. Reactive oxygen species in the neuropathogenesis of hypertension. *Curr Hypertens Rep* 8: 232–241, 2006.
100. Pilowsky P, Goodchild AK. Baroreceptor reflex pathways and neurotransmitters: 10 years on. *J Hypertens* 20: 1675–1688, 2002.
101. Plochocka-Zulinska D, Krukoff TL. Increased gene expression of neuronal nitric oxide synthase in brain of adult spontaneously hypertensive rats. *Mol Brain Res* 48: 291–297, 1997.
102. Polizio AH, Peña C. Effects of angiotensin II type 1 receptor blockade on the oxidative stress in spontaneously hypertensive rat tissues. *Regul Pept* 128: 1–5, 2005.
103. Pontieri V, Venezuela MK, Scavone C, Michelini LC. Role of endogenous nitric oxide in the nucleus tractus solitarius on baroreflex control of heart rate in spontaneously hypertensive rats. *J Hypertens* 16: 1993–1999, 1998.
104. Qadri F, Arens T, Schwarz EC, Häuser W, Dendorfer A, Dominiak P. Brain nitric oxide synthase activity in spontaneously hypertensive rats during development of hypertension. *J Hypertens* 21: 1687–1694, 2003.
105. Reja V, Goodchild AK, Phillips JK, Pilowski PM. Upregulation of angiotensin AT<sub>1</sub> receptor and intracellular kinase gene expression in hypertensive rats. *Clin Exp Pharmacol Physiol* 33: 690–695, 2006.
106. Ren J. Influence of gender on oxidative stress, lipid peroxidation, protein damage and apoptosis in hearts and brains from spontaneously hypertensive rats. *Clin Exp Pharmacol Physiol* 34: 432–438, 2007.
107. Sakai K, Hirooka Y, Matsuo I, Eshima K, Shigematsu H, Shimokawa H, Takeshita A. Overexpression of eNOS in NTS causes hypotension and bradycardia in vivo. *Hypertension* 36: 1023–1028, 2000.
108. Sakai K, Agassandian K, Morimoto S, Sinnayah P, Cassell MD, Davisson RL, Sigmund CD. Local production of angiotensin II in the subfornical organ causes elevated drinking. *J Clin Invest* 117: 1088–1095, 2007.
109. Sander M, Chavoshan B, Victor RG. A large blood pressure-raising effect of nitric oxide synthase inhibition in humans. *Hypertension* 33: 937–942, 1999.
110. Sano H, Matsumoto K, Utsumi H. Synthesis and imaging of blood-brain-barrier permeable nitroxyl-probes for free radicals reactions in brain of living mice. *Biochem Mol Biol Int* 42: 641–647, 1997.
111. Sano H, Naruse M, Matsumoto K, Oi T, Utsumi H. A new nitroxyl-probe with high retention in the brain and its application for brain imaging. *Free Radic Biol Med* 28: 959–969, 2000.
112. Shapoval LN, Sagach VF, Pobegailo LS. Nitric oxide influences ventrolateral medullary mechanisms of vasomotor control in the cat. *Neurosci Lett* 132: 47–50, 1991.
113. Sun C, Sellers KW, Summers C, Raizada MK. NAD(P)H oxidase inhibition attenuates neuronal chronotropic actions of angiotensin II. *Circ Res* 96: 659–666, 2005.
114. Sun J, Druhan LJ, Zweier JL. Reactive oxygen and nitrogen species regulate inducible nitric oxide synthase function shifting the balance of nitric oxide and superoxide production. *Arch Biochem Biophys* 494: 130–137, 2010.
115. Sved AF, Ito S, Sved JC. Brainstem mechanisms of hypertension: role of the rostral ventrolateral medulla. *Curr Hypertens Rep* 5: 262–268, 2003.
116. Tagawa T, Imaizumi T, Harada S, Endo T, Shiramoto M, Hirooka Y, Takeshita A. Nitric oxide influences neuronal activity in the nucleus tractus solitarius of rat brainstem slices. *Circ Res* 75: 70–76, 1994.
117. Tai MH, Wang LL, Wu KLH, Chan JYH. Increased superoxide anion in rostral ventrolateral medulla contributes to hypertension in spontaneously hypertensive rats via interactions with nitric oxide. *Free Radic Biol Med* 38: 450–462, 2005.
118. Talman WT, Dragon DN. Transmission of arterial baroreflex signals depends on neuronal nitric oxide synthase. *Hypertension* 43: 820–824, 2004.
119. Talman WT. NO and central cardiovascular control: a simple molecule with a complex story. *Hypertension* 48: 552–554, 2006.
120. Tseng CJ, Liu HY, Lin HC, Ger LP, Tung CS, Yen MH. Cardiovascular effects of nitric oxide in the brain stem nuclei of rats. *Hypertension* 27: 36–42, 1996.
121. Waki H, Murphy D, Yao ST, Kasparov S, Paton JFR. Endothelial NO synthase activity in nucleus tractus solitarius contributes to hypertension in spontaneously hypertensive rats. *Hypertension* 48: 644–650, 2006.
122. Wang G, Anrather J, Huang J, Speth RC, Pickel VM, Iadecola C. NADPH oxidase contributes angiotensin signaling in the nucleus tractus solitarius. *J Neurosci* 24: 5516–5524, 2004.
123. Wang G, Anrather J, Glass MJ, Tarsitano J, Zhou P, Frys KA, Pickel VM, Iadecola C. Nox2, Ca<sup>2+</sup>, and protein kinase C play a role in angiotensin II-induced free radical production in nucleus tractus solitarius. *Hypertension* 48: 482–489, 2006.
124. Wang JM, Tan J, Leenen FHH. Central nervous system blockade by peripheral administration of AT<sub>1</sub> receptor blockers. *J Cardiovasc Pharmacol* 41: 593–599, 2003.
125. Wang S, Paton JFR, Kasparov S. Differential sensitivity of excitatory and inhibitory synaptic transmission to modulation by nitric oxide in rat nucleus tractus solitarius. *Exp Physiol* 92: 371–382, 2007.
126. Wu SY, Dun NJ. Potentiation of IPSCs by nitric oxide in immature rat sympathetic preganglionic neurons in vitro. *J Physiol* 495: 479–490, 1996.
127. Wu SY, Dun NJ. Nitric oxide and excitatory postsynaptic currents in immature rat sympathetic preganglionic neurons in vitro. *Neuroscience* 79: 237–247, 1997.
128. Yin JX, Yang RF, Li S, Renshaw AO, Li YL, Schultz HD, Zimmerman MC. Mitochondria-produced superoxide mediates angiotensin II-induced inhibition of neuronal potassium current. *Am J Physiol Cell Physiol* 298: C857–C865, 2010.
129. Zanzinger J. Role of nitric oxide in the neural control of cardiovascular function. *Cardiovasc Res* 43: 639–649, 1999.
130. Zanzinger J. Mechanisms of action of nitric oxide in the brain stem: role of oxidative stress. *Auton Neurosci* 98: 24–27, 2002.
131. Zanzinger J, Czachurski J, Seller H. Inhibition of basal and reflex-mediated sympathetic activity in the RVLM by nitric oxide. *Am J Physiol Regul Integr Comp Physiol* 268: R958–R962, 1995.
132. Zimmerman MC, Lazartigues E, Lang JA, Sinnayah P, Ahmad IM, Spitz DR, Davisson RL. Superoxide mediates the actions of angiotensin II in the central nervous system. *Circ Res* 91: 1038–1045, 2002.
133. Zimmerman MC, Lazartigues E, Sharma RV, Davisson RL. Hypertension caused by angiotensin II infusion involves increased superoxide production in the central nervous system. *Circ Res* 95: 210–216, 2004.
134. Zimmerman MC, Dunlay RP, Larzartigues E, Zhang Y, Sharma RV, Engelhardt JF, Davisson RL. Requirement for Rac-1-dependent NADPH oxidase in the cardiovascular and dipsogenic actions of angiotensin II in the brain. *Circ Res* 95: 532–539, 2004.
135. Zimmerman MC, Sharma RV, Davisson RL. Superoxide mediates angiotensin II-induced influx of extracellular calcium in neural cells. *Hypertension* 45: 717–723, 2005.
136. Zimmerman MC, Zucker IH. Mitochondrial dysfunction and mitochondrial-produced reactive oxygen species: new targets for neurogenic hypertension? *Hypertension* 53: 112–114, 2009.

# Pulmonary Hypertension

## Nanoparticle-Mediated Delivery of Pitavastatin Into Lungs Ameliorates the Development and Induces Regression of Monocrotaline-Induced Pulmonary Artery Hypertension

Ling Chen, Kaku Nakano, Satoshi Kimura, Tetsuya Matoba, Eiko Iwata, Miho Miyagawa, Hiroyuki Tsujimoto, Kazuhiro Nagaoka, Junji Kishimoto, Kenji Sunagawa, Kensuke Egashira

**Abstract**—Pulmonary artery hypertension (PAH) is an intractable disease of the small PAs in which multiple pathogenic factors are involved. Statins are known to mitigate endothelial injury and inhibit vascular remodeling and inflammation, all of which play crucial roles in the pathogenesis of PAH. We tested the hypothesis that nanoparticle (NP)-mediated delivery of pitavastatin into the lungs can be a novel therapeutic approach for the treatment of PAH. Among the marketed statins, pitavastatin was found to have the most potent effects on proliferation of PA smooth muscle cells in vitro. We formulated pitavastatin-NP and found that pitavastatin-NP was more effective than pitavastatin alone in inhibiting cellular proliferation and inflammation in vitro. In a rat model of monocrotaline-induced PAH, a single intratracheal instillation of NP resulted in the delivery of NP into alveolar macrophages and small PAs for up to 14 days after instillation. Intratracheal treatment with pitavastatin-NP, but not with pitavastatin, attenuated the development of PAH and was associated with a reduction of inflammation and PA remodeling. NP-mediated pitavastatin delivery was more effective than systemic administration of pitavastatin in attenuating the development of PAH. Importantly, treatment with pitavastatin-NP 3 weeks after monocrotaline injection induced regression of PAH and improved survival rate. This mode of NP-mediated pitavastatin delivery into the lungs is effective in attenuating the development of PAH and inducing regression of established PAH, suggesting potential clinical significance for developing a new treatment for PAH. (*Hypertension*. 2011;57:343-350.) • **Online Data Supplement**

**Key Words:** pulmonary hypertension ■ nanotechnology ■ pitavastatin ■ inflammation ■ leukocytes

Pulmonary artery hypertension (PAH) is an intractable disease of the small PAs resulting in progressive increases in pulmonary vascular resistance, right ventricular (RV) failure, and ultimately premature death.<sup>1,2</sup> Mortality from PAH remains high, even after introduction of vasodilator therapies such as prostacyclin infusion, endothelin receptor antagonists, and phosphodiesterase inhibitors (which have raised the 5-year survival rate to ≈50%). Although these drugs were originally developed for non-PAH vascular diseases, they were introduced into treatment for clinical PAH on the basis of the vasodilator hypothesis. Therefore, a new idea that might lead to a breakthrough curative treatment for PAH is urgently needed.

In addition to vasoconstriction, other multiple factors (endothelial injury/apoptosis, obstructive vascular remodeling, proliferation, and inflammation) play an important role in the mechanism of PAH.<sup>1,2</sup> Therefore, we hypothesized that a controlled, local delivery system targeting a battery of those pathogenic factors intrinsic to PAH pathology would be a favorable therapeutic approach with high translational poten-

tial to clinical medicine. In this respect, we focused on the vasculoprotective effects of 3-hydroxy-3-methylglutaryl coenzyme A reductase inhibitors, the so-called statins. Statins are known to increase expression and activity of endothelial nitric oxide synthase (eNOS) and thus ameliorate endothelial injury.<sup>3-6</sup> Prior studies have reported that systemic administration of statins attenuates monocrotaline (MCT)-induced and hypoxia-induced PAH in animals.<sup>7-9</sup> These beneficial therapeutic effects of statins on PAH, however, were observed after daily administration of high doses of statins, a regimen that could lead to serious adverse side effects in the clinical setting. However, not all studies have reported beneficial effects of statins with regard to PAH in animal models.<sup>10,11</sup> We recently reported that (1) intratracheal administration of bioabsorbable polymeric nanoparticles (NPs) represented a novel drug delivery system into the lung; and (2) NP-mediated delivery of a nuclear factor (NF)- $\kappa$ B decoy into the lungs effectively inhibited NF- $\kappa$ B-mediated inflammation and thus, attenuated the development and progression of PAH in a rat model of MCT-induced PAH.<sup>12</sup> This

Received May 23, 2010; first decision June 21, 2010; revision accepted December 8, 2010.

From the Department of Cardiovascular Medicine (L.C., K.N., T.M., E.I., M.M., K.N., K.S., K.E.) and Digital Medicine Initiative (J.K.), Graduate School of Medical Science, Kyushu University, Fukuoka, and Hosokawa Micron Corporation (H.T.), Osaka, Japan.

Correspondence to Kensuke Egashira, Department of Cardiovascular Medicine, Graduate School of Medical Science, Kyushu University, 3-1-1, Maidashi, Higashi-ku, Fukuoka 812-8582, Japan. E-mail [egashira@cardiol.med.kyushu-u.ac.jp](mailto:egashira@cardiol.med.kyushu-u.ac.jp)

© 2011 American Heart Association, Inc.

*Hypertension* is available at <http://hyper.ahajournals.org>

DOI: 10.1161/HYPERTENSIONAHA.110.157032

nanotechnology platform may optimize the efficacy and minimize the potential side effects of drugs.

Therefore, the primary aim of this study was to test the hypothesis that NP-mediated local delivery of statins to the lung is an innovative therapeutic approach for PAH. Pitavastatin was selected as the nanoparticulation compound because this drug has shown the most potent beneficial effects on human endothelial and smooth muscle cells *in vitro* compared with other statins.<sup>13,14</sup> We then used a rat model of MCT-induced PAH and examined (1) whether this NP-mediated delivery of pitavastatin into the lung is more effective than intratracheal or systemic administration of pitavastatin in attenuating the development of PAH and (2) whether this NP-mediated delivery system induces regression of established PAH.

## Materials and Methods

### Human PA Smooth Muscle Cell Proliferation Assay

Human PA smooth muscle cells (PASMCs) were seeded on 96-well culture plates at  $10^4$  cells per well in SmBM. After 24 hours of starvation, 10% fetal bovine serum was added for cell stimulation. In addition, various concentrations of statins (simvastatin, pitavastatin, atorvastatin, losuvastatin, fluvastatin, and pravastatin) or vehicle were added ( $n=6$  per group). Statins were purchased, extracted from products, and purified. Cells were incubated for another 24 hours after addition of 5'-bromo-2'-deoxyuridine, and 5'-bromo-2'-deoxyuridine incorporation was evaluated by an ELISA kit from Calbiochem.

In another set of experiments, a 1.0-mL suspension of pitavastatin at 5 mg/mL, fluorescein isothiocyanate (FITC)-NP (1 mg/mL lactide/glycolide copolymer [PLGA]), pitavastatin-NP containing 1.0 mg/mL PLGA and 5 mg/mL pitavastatin, or vehicle was added to each well ( $n=6$  per group). Cells were incubated for another 4 days, and the cells were fixed with methanol and stained with Diff-Quick staining solution. A single observer counted the number of cells per plate.

### Preparation of PLGA-NP

A PLGA with an average molecular weight of 20 000 and a copolymer ratio of lactide to glycolide of 75:25 (Wako Pure Chemical Industries, Osaka, Japan) was used as wall material for the NP. PLGA-NP incorporated with FITC or pitavastatin (Kowa Pharmaceutical Co Ltd, Tokyo, Japan) was prepared by a previously reported emulsion solvent diffusion method in purified water.<sup>15,16</sup> PLGA was dissolved in a mixture of acetone and methanol. Then, FITC or pitavastatin was added to this solution. The resultant PLGA-FITC or PLGA-statin solution was emulsified in a polyvinyl alcohol solution with stirring at 400 rpm by using a propeller-type agitator with 3 blades (Heidon 600G, Shinto Scientific, Tokyo, Japan). After the system was agitated for 2 hours under reduced pressure at 40°C, the entire suspension was centrifuged (20 000g for 20 minutes at -20°C). After the supernatant was removed, purified water was added and mixed with the sediment. The wet mixture was then centrifuged again to remove the excess polyvinyl alcohol and the unencapsulated reagent that could not adsorb onto the surfaces of the NPs. After this process was repeated, the resultant dispersion was freeze-dried under the same conditions. The FITC- and pitavastatin-loaded PLGA-NP contained 13% (wt/vol) FITC and 13% (wt/vol) pitavastatin, respectively. A sample of NP suspension in distilled water was used for particle size analysis. The diameter of NPs was  $196\pm 29$  nm. Surface charge (zeta potential) was also analyzed by Zetasizer Nano (Sysmex, Hyogo, Japan) and was anionic ( $-15\pm 10$  mV at pH 4.4).

### Experimental Animal Models

All experiments were reviewed and approved by the committee on ethics on animal experiments, Kyushu University Faculty of Medicine, and were conducted according to the guidelines of the American Physiological Society. Adult male Sprague-Dawley rats (Charles River, Yokohama, Japan; 250 to 300 g body weight) were injected subcutaneously with 60 mg/kg MCT (Wako), which induces severe PAH in 3 weeks.<sup>12,17</sup>

In a prevention protocol, animals were divided into 4 groups that received intratracheal instillation of phosphate-buffered saline (PBS), pitavastatin only (100  $\mu$ g), FITC-NP (1 mg PLGA), or pitavastatin-NP (100  $\mu$ g pitavastatin per mg PLGA) immediately after MCT injection. For intratracheal instillation, a 0.1-mL suspension of pitavastatin, FITC-NP, or pitavastatin-NP was injected gently into the trachea of animals, accompanied by an equal volume of air. This dose of pitavastatin was selected because we examined the effects of intratracheal instillation of various concentrations and volumes of pitavastatin suspension (10, 30, 100, or 300  $\mu$ g per animal in 0.05, 0.1, and 0.2 mL PBS) and confirmed that a 0.1-mL suspension of pitavastatin containing 100  $\mu$ g pitavastatin was an optimal dose in our experiments. In a treatment protocol, rats were divided into 4 groups that received intratracheal instillation of PBS, pitavastatin only (100  $\mu$ g), FITC-NP (1 mg PLGA), or pitavastatin-NP (100  $\mu$ g pitavastatin per mg PLGA) 21 days after MCT injection when severe PAH had already been established. In another set of experiments, 3 other groups received systemic daily oral pitavastatin at doses of 0.3, 1.0, 3.0, and 10 mg/kg, dissolved in 0.5% carboxymethyl cellulose, by gavage from the day of MCT injection until the mice were euthanized on day 21.

### Biodistribution of FITC-NP After Intratracheal Administration Into the Lung

Biodistribution of FITC in the lung was examined in rats that received intratracheal instillation of FITC-NP. Animals were euthanized and the tracheas were exposed. The lungs were inflated with a solution of 10% phosphate-buffered formalin (pH 7.4) by using a catheter inserted into the trachea. The lungs were then removed en bloc and placed into 10% phosphate-buffered formalin for a further 12 to 18 hours. After light and fluorescence stereoscopic photographs of the lungs were taken, the tissues were processed and embedded in OCT compound, and cross sections of 5- $\mu$ m thickness were prepared for detecting NP distribution by fluorescence photomicroscopy. The tissue specimens were also processed and embedded in paraffin according to standard procedures, and 5- $\mu$ m sections were cut. Sections were further examined to detect NP distribution by immunostaining.

### Direct RV Pressure Measurements

Three weeks after MCT administration, the animals were anesthetized with sodium pentobarbital, and polyethylene catheters were then inserted into the right ventricle through the jugular vein and carotid artery for hemodynamic measurements. RV systolic pressure and systemic blood pressure were measured with a polygraph system (AP-601G, Nihon Kohden).<sup>12,17</sup>

### Echocardiographic Measurements of RV and PA Hemodynamics

Transthoracic echocardiographic measurements (Vevo 2100 ultrasound system; Primetech Inc) were performed as described previously.<sup>18</sup> Additional details are provided in the online-only Data Supplement (available at <http://hyper.ahajournals.org>).

### Assessment of Right Heart Hypertrophy and PA Remodeling

After systemic arterial and RV pressures were recorded, the animals were euthanized and the lungs and heart were isolated. The RV wall was dissected from the left ventricle and ventricular septum. Wet weight of the right ventricle and of the left ventricle plus ventricular

septum was determined, and RV hypertrophy was expressed as RV weight/(left ventricle plus ventricular septum weights).<sup>12,17</sup>

The lungs were perfused with a solution of 10% phosphate-buffered formalin (pH 7.4). At the same time, 10% phosphate-buffered formalin (pH 7.4) was administered into the lungs via tracheal tube at a pressure of 20 cm H<sub>2</sub>O. These specimens were processed for light microscopy by routine paraffin embedding. The degree of remodeling (muscularization) of small, peripheral, PAs was assessed by double immunohistochemical staining of the 5- $\mu$ m sections with an anti- $\alpha$ -smooth muscle actin antibody (dilution 1:500; clone 1A4, Dako) and anti-platelet endothelial cell adhesion molecule-1 (PECAM-1) (M-20) antibody (dilution 1:100, Santa Cruz).<sup>12</sup> To assess the type of remodeling of muscular PAs, microscopic images were analyzed. In each rat, 30 to 40 intra-acinar arteries were categorized as muscular (those with a complete medial coat of muscle), partially muscular (those with only a crescent of muscle), or nonmuscular (those with no apparent muscle), counted, and averaged within a range of diameters from 25 to 50  $\mu$ m.<sup>12</sup>

### Histopathologic and Immunohistochemical Analysis of Rat Lungs

The degrees of monocyte infiltration were evaluated by immunostaining for ED-1 (analog of human CD68, Serotec). For quantification, a blinded observer counted the number of ED-1-positive cells in 10 fields. Sections were also subjected to immunostaining with antibodies against FITC (1:1000; American Research Products, Belmont, MA), an epitope ( $\alpha$ -p65) on the p65 subunit of NF- $\kappa$ B (1:100; Boehringer Mannheim, Roche Diagnostics, Basel, Switzerland), rabbit eNOS (ABR: PA1-037), murine inducible NOS (iNOS, Transduction Laboratories), or nonimmune mouse IgG (Dako). The  $\alpha$ -p65 monoclonal antibody recognizes an epitope on the p65 subunit that is masked by bound inhibitor- $\kappa$ B.<sup>19</sup> Therefore, this antibody exclusively detects activated NF- $\kappa$ B.<sup>19</sup>

### Real-Time Quantitative Reverse Transcription-Polymerase Chain Reaction

Real-time polymerase chain reaction amplification was performed with rat cDNA with the use of an ABI PRISM 7000 sequence detection system (Applied Biosystems, Foster City, CA) as described previously.<sup>12,19</sup> TaqMan primers/probes for monocyte chemoattractant protein-1, tumor necrosis factor- $\alpha$ , interleukin (IL)-1 $\beta$ , IL-6, intercellular adhesion molecule-1, and glyceraldehyde 3-phosphate dehydrogenase, which served as the endogenous reference, were purchased from Applied Biosystems (Assay-on-Demand gene expression products Rn00580555, Rn99999017, Rn00580432, Rn00561420, and Rn00564227 and TaqMan rodent glyceraldehyde 3-phosphate dehydrogenase control reagents, respectively).

### Lipopolysaccharide-Induced Activation of Mouse Monocytes

The mouse macrophage cell line RAW 264.7 was purchased. After bacterial lipopolysaccharide (serotype 0111:B4, Sigma) at 1  $\mu$ g/mL was added to the cells, each 1.0-mL suspension of pitavastatin at 5 mg/mL, FITC-NP (1 mg/mL PLGA), pitavastatin-NP containing 1.0 mg/mL PLGA and 5 mg/mL pitavastatin, or vehicle was added to the wells; 2 hours later, the cells were washed 3 times with PBS. NF- $\kappa$ B pathway activity was measured with a TransAM NF- $\kappa$ B p65 ELISA-based assay kit (Active Motif, Tokyo, Japan). Nuclear extracts of RAW 264.7 cells were prepared with the NE-PER nuclear and cytoplasmic extraction reagent kit (Pierce, Rockford, IL) according to the manufacturer's protocol. Samples were placed, along with 30  $\mu$ L of binding buffer, on a 96-well plate to which oligonucleotides containing an NF- $\kappa$ B consensus binding site had been immobilized for 1 hour on a shaker. During this time, the activated NF- $\kappa$ B contained in the sample specifically binds to this nucleotide; then the plate was washed and, by using a primary antibody (100 mL diluted 1:1000 in antibody binding buffer for 1 hour) that is directed against the NF- $\kappa$ B p65 subunit, the NF- $\kappa$ B complex bound to the oligonucleotides can be detected. The plate was then washed again, and 100  $\mu$ L of secondary antibody (diluted 1:1000 in antibody binding

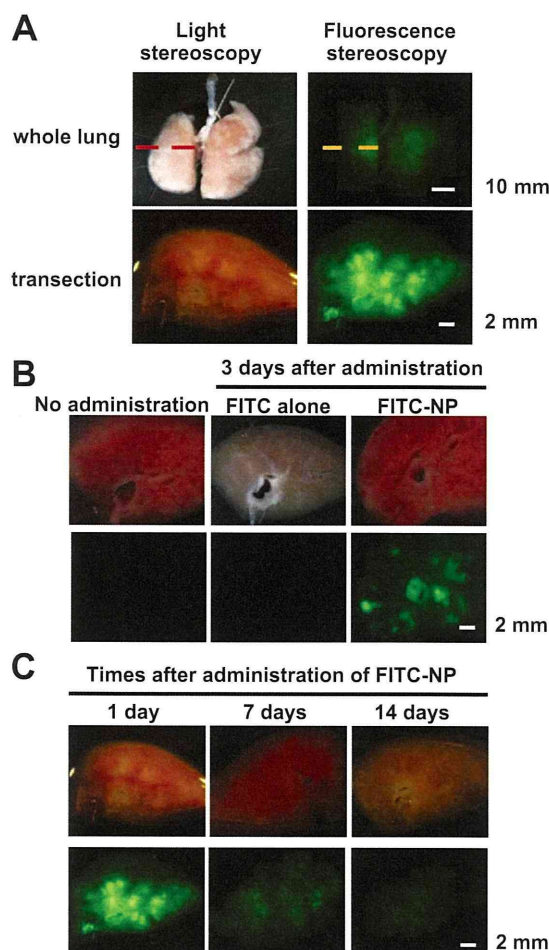


**Figure 1.** Localization of FITC-NP after instillation into the rat lung. A, Representative light (left) and fluorescence (right) stereomicrographs of whole lungs (upper) and transections (lower) 1 hour after intratracheal instillation of FITC-NP. B, Representative light (upper) and fluorescence (lower) stereomicrographs of transections from control (nontreated) lungs and from lungs instilled with FITC alone or FITC NP on day 3 after instillation. C, Representative light (upper) and fluorescence (lower) stereomicrographs of cross sections from lungs instilled with FITC-NP on days 1, 7, and 14 after instillation.

buffer) conjugated to horseradish peroxidase was added for 1 hour. The plate was washed again, and 100  $\mu$ L of developing solution was added. The plate was incubated for 4 minutes away from direct light, 100  $\mu$ L of stop solution was added, and the plate was read with a plate reader at 450 nm.

### Western Blot Analysis

Protein was extracted from frozen lung tissues. Samples were homogenized in lysis buffer containing 10 mmol/L Tris-HCl, pH 7.4, 50 mmol/L NaCl, 5 mmol/L EDTA, 1% Triton X-100, 50 mmol/L NaCl, 30 mmol/L sodium phosphate, 50 mmol/L NaF, 1% aprotinin, 0.5% pepstatin A, 2 mmol/L phenylmethylsulfonyl fluoride, and 5 mmol/L leupeptin and phosphatase inhibitor cocktail (Pierce). Cell lysates (50  $\mu$ g) were separated on 7.5% polyacrylamide gels and blotted onto polyvinylidene difluoride membranes (Millipore Co, Hercules, CA). Protein expression was analyzed by using antibodies against eNOS (ABR: PA1-037) or actin (Sigma). Immune complexes were visualized with horseradish peroxidase-conjugated secondary antibodies. Bound antibodies were detected by chemiluminescence with the use of an ECL detection system (Amersham Biosciences) and quantified by densitometry.



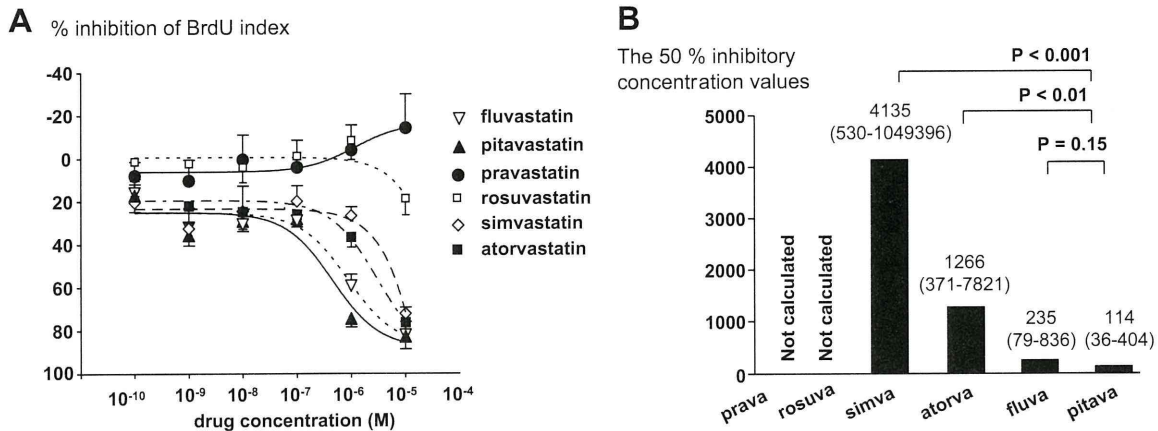


**Figure 2.** Inhibitory effects of various statins on human PASC proliferation. A, PASC proliferation assay (% inhibition of 5'-bromo-2'-deoxyuridine [BrdU] index) in response to various concentrations of various statins (n=6 per group). B, IC<sub>50</sub> values and 95% Wald CIs (in parentheses) are shown at the top of each bar. Probability values vs pitavastatin by Wald tests in a 4-parameter logistic-regression model are shown. Prava indicates pravastatin; rosuva, rosuvastatin; simva, simvastatin; atorva, atorvastatin; fluva, fluvastatin; and pitava, pitavastatin.

### Measurements of Pitavastatin Concentration

Pitavastatin concentrations in serum and lung were measured at predetermined time points by using a column-switching high-performance liquid chromatography system, as previously reported.<sup>20</sup> In brief, the column-switching high-performance liquid chromatography system consists of 2 LC-10AD pumps, an SIL-10A autosampler, a CTO-10A column oven, a 6-port column-switching valve, and an SPD-10A UV detector (all from Shimadzu, Kyoto, Japan). The column temperature was maintained at 40°C. Prepared serum or tissue homogenate sample solutions were injected from the autosampler into the high-performance liquid chromatography system, and detection of the statin in sample solutions was performed at 250 nm with a UV detector. The detected peak area was measured with Lcsolution software (Shimadzu).

### Statistical Analysis

Data are presented as mean ± SEM. Statistical analysis of differences was performed by 1-way ANOVA and Bonferroni's multiple comparison tests. The survival rates were determined by the Kaplan-Meier method. Efficacy ratios (median inhibitory concentration [IC<sub>50</sub>] values) of statins were tested with Wald tests in a 4-parameter logistic-regression model. Point estimates and Wald 95% CIs for IC<sub>50</sub> values were calculated. Statistical calculations were performed with SAS preclinical package software version 9.1.3 (SAS Institute Inc, Tokyo, Japan) and Prism Software version 4.0.1 (GraphPad). A value of  $P < 0.05$  was considered statistically significant.

## Results

### Localization of FITC-NP in the Lung of Rats With MCT-Induced PAH

Localization of FITC was examined after a single intratracheal instillation of FITC-NP into animals injected with MCT. Three days after instillation, strong FITC signals were detected only in FITC-NP-instilled lungs, whereas no or only faint FITC signals were observed in control noninjected lungs and in lungs injected with FITC only (Figure 1). On days 1, 7, and 14, FITC signals remained localized predominantly in the lungs. There were FITC-positive cells in the bronchi and alveoli, alveolar macrophages, and small arteries. As we previously reported,<sup>12</sup> immunofluorescence staining revealed that FITC signals localized mainly in small arteries and arterioles as well as in small bronchi and alveoli 14 days

after instillation of FITC-NP (online-only Figure I). FITC signals were not detected in remote organs (liver, spleen, and heart) at any time point (data not shown).

### Inhibitory Effects of Statins on Human PASC Proliferation

To implicate pitavastatin as a candidate statin for nanoparticulation, the effects of statins on PASC proliferation were examined. In a human PASC proliferation assay (percent inhibition of 5'-bromo-2'-deoxyuridine index), hydrophilic statins (rosuvastatin and pravastatin) elicited no inhibitory effects, whereas other statins showed dose-dependent effects (Figure 2A). The IC<sub>50</sub> value of pitavastatin was lower than that of simvastatin or atorvastatin (Figure 2B). The IC<sub>50</sub> value of pitavastatin tended to be lower than that of fluvastatin, but there was no significant difference in the IC<sub>50</sub> values between the 2 statins.

### Effects of Pitavastatin-NP on the Development of PAH in the Rat Model of MCT-Induced PAH

An RV catheterization study confirmed that injection of MCT led to severe PAH (increased RV systolic pressure) associated with small PA remodeling and increased infiltration of ED1-positive monocytes 3 weeks after MCT injection, as previously reported.<sup>12,17</sup> Single intratracheal treatment with pitavastatin-NP, but not with pitavastatin alone or FITC-NP, attenuated the development of PAH, small PA remodeling, and monocyte-mediated inflammation (Figure 3). The RV systolic pressure of untreated normal controls (no MCT injection) was 34 ± 2 mm Hg (n=10). There were no significant differences in concentrations of pitavastatin in the lung and systemic blood between pitavastatin-NP-treated and pitavastatin-only groups (the Table).

Echocardiographic study showed that there were no significant changes in cardiac output or stroke volume among untreated control and MCT-induced PAH rats (online-only Table I). Echo-derived estimation of RV systolic pressure and pulmonary vascular resistance showed the development of MCT-induced PAH and therapeutic effects of a single intra-

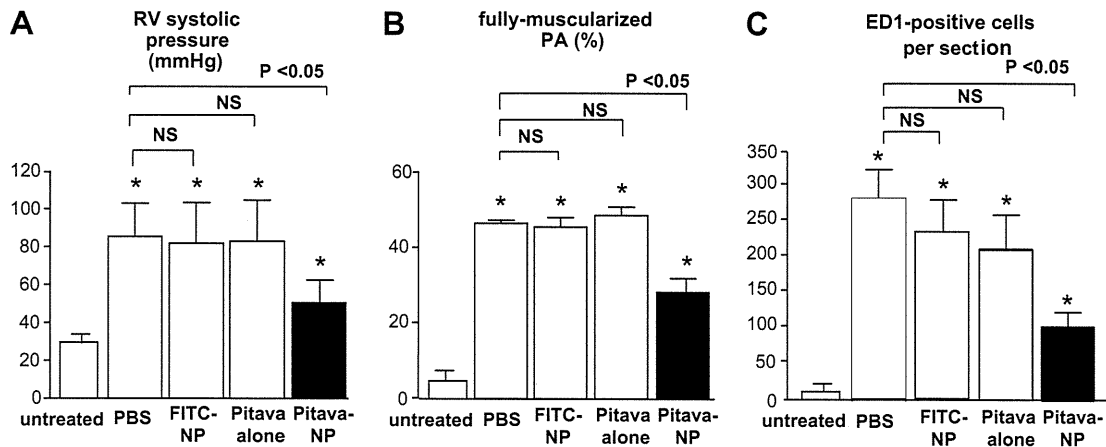


**Figure 3.** Effects of pitavastatin (pitava)-NP on RV systolic pressure, small PA remodeling, and infiltration of monocytes 3 weeks after MCT injection. A, RV systolic pressure in the 4 experimental groups. Data are mean±SEM (n=6 per group). B, Percentage of fully muscularized small PAs in the 4 experimental groups. Data are mean±SEM (n=6 per group). C, Infiltration of ED1-positive monocytes into the lung (the number of positive cells per 30 high-power-field cross sections). Data are mean±SEM (n=6 per group). \*P<0.01 vs untreated control.

tracheal instillation of pitavastatin-NP, as reported by the RV catheterization study.

The activity of lactate dehydrogenase was not detected in bronchoalveolar lavage fluid. There were no significant changes in activity of lactate dehydrogenase and various biomarkers in lung tissue homogenates among untreated control and MCT-induced PAH rats (online-only Tables II and III).

Oral daily administration of pitavastatin at 0.3 mg/kg had no significant effects on MCT-induced PAH, but pitavastatin at 1.0, 3.0, and 10 mg/kg significantly attenuated the development of PAH (online-only Figure II).

**Effects of Intratracheal Instillation of Pitavastatin-NP on NF-κB Activation and PAMSC Proliferation**

As previously reported,<sup>12</sup> immunohistochemically detectable NF-κB activation was noted mainly in alveolar macrophages and weakly in PA lesions 7 days after MCT administration (Figure 4). A single intratracheal instillation of pitavastatin-NP, but not of FITC-NP or pitavastatin alone, markedly

**Table. Pitavastatin Concentrations in the Lung and Systemic Blood After Intratracheal Administration of Pitavastatin (100 μg per Animal) Only or Pitavastatin-NP Containing the Same Dose of Pitavastatin**

Groups	Time After Administration, h					
	1	3	6	12	24	48
<b>Pitavastatin-only group</b>						
Lung, ng/g	115±83	49±69	7±5	2±1	3±3	4±3
Serum, ng/mL	48±19	24±10	9±7	1±1	1±1	1±1
<b>Pitavastatin-NP group</b>						
Lung, ng/g	155±77	17±8	13±13	4±6	7±4	3±1
Serum, ng/mL	65±19	20±5	7±4	2±1	1±1	1±2

Data are mean±SEM (n=6 per group).

attenuated the increases in NF-κB (α-p65) activity induced by MCT injection (Figure 4). Because NF-κB was activated in alveolar monocytes in MCT-induced PAH, effects of pitavastatin-NP on NF-κB activity were examined in a monocyte cell line (RAW 264.7 cells) in vitro. Treatment with pitavastatin-NP, but not with pitavastatin only, attenuated NF-κB activation in RAW 264.7 cells (online-only Figure III). Because proliferation of PAMSCs is increased in animals and humans with PAH, effects of pitavastatin and pitavastatin-NP were examined in human PAMSCs in vitro. Treatment with pitavastatin-NP, but not with pitavastatin only, attenuated the proliferation of PAMSCs (online-only Figure IV).

**Effects of Pitavastatin-NP on Expression of Proinflammatory Factors**

As previously reported,<sup>12</sup> MCT-induced PAH was associated with increased gene expression of proinflammatory factors. Intratracheal treatment with pitavastatin-NP significantly reduced the increased gene expression of monocyte chemotactic protein-1, tumor necrosis factor-α, and IL-6 and tended to decrease the expression of IL-1β and intercellular adhesion molecule-1 (online-only Figure V).

**Effects of Pitavastatin-NP on eNOS and iNOS Expression**

Because the protective effects of statins on PAH have been reported to be attributable at least to the eNOS-related pathway,<sup>11</sup> eNOS protein expression in the lungs was examined on days 3 and 21 after treatment. Western blot analysis showed that MCT administration had no significant effect on eNOS expression on days 3 and 21, compared with untreated controls (Figure 5). Pitavastatin-NP, but not FITC-NP or pitavastatin alone, increased the protein expression of eNOS on day 3, whereas pitavastatin-NP showed no therapeutic effects on eNOS expression on day 21 (Figure 5).

In contrast, iNOS is known to cause oxidant tissue injury and accelerates the pathologic processes of PAH.<sup>21</sup> Immuno-

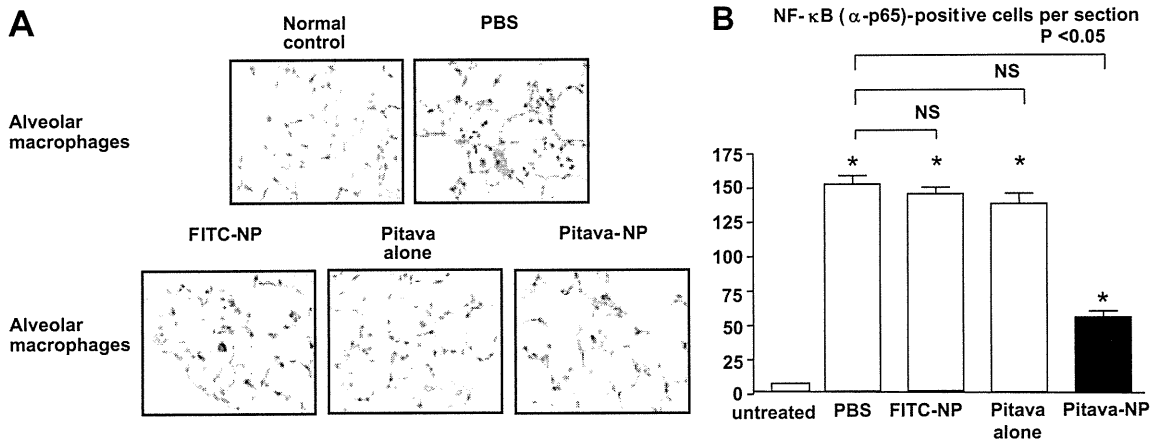


**Figure 4.** Effects of pitavastatin (pitava)-NP on NF-κB activation. A, Photomicrographs of cross sections of lung stained immunohistochemically with NF-κB (α-p65) from normal rats and PAH rats 3 days after MCT injection. B, Effects of pitavastatin-NP on infiltration of NF-κB (α-p65)-positive cells 3 days after MCT injection. Data are mean±SEM (n=6 per group). \*P<0.01 vs untreated control.

histochemical expression of iNOS was not detected in lung sections from untreated control rats. Immunostaining for iNOS was noted mainly in alveolar macrophage and weakly in PA lesions 3 days after MCT administration (online-only Figure VI). Single intratracheal instillation of pitavastatin-NP, but not of FITC-NP or pitavastatin only, markedly

attenuated the increase in iNOS activity induced by MCT injection.

**Effects of Pitavastatin-NP on Survival**

In the treatment protocol, pitavastatin-NP significantly improved survival rate: 42% in the PBS group (n=40), 39% in the FITC-NP group (n=33), 40% in the pitavastatin-alone group (n=40), and 64% in the pitavastatin-NP group (n=58; Figure 6). In addition, pitavastatin-NP caused regression of MCT-induced PAH (Figure 6).

**Discussion**

We recently reported that intratracheal instillation of a polyethylene glycol-*block*-PLGA copolymer (PEG-PLGA) is an excellent system for drug delivery to the lung.<sup>12</sup> We found in the present study that PLGA NPs were as effective as PEG-PLGA NPs as an NP-mediated drug delivery system to the lung. As we reported with PEG-PLGA NPs,<sup>12</sup> the FITC signals were detected in small bronchial tracts, alveolar macrophages, and small PAs for up to 14 days after a single instillation of FITC-encapsulated PLGA NP.

Statins are known to ameliorate the effects of endothelial injury/dysfunction by enhancing the activity of eNOS and thus, exert multiple vasculoprotective effects on other cell types (vascular smooth muscle cells, monocytes, etc).<sup>3-5</sup> We recently reported that NP-mediated pitavastatin delivery to the vascular endothelium of ischemic skeletal muscles effectively increased therapeutic neovascularization in a murine model of hindlimb ischemia.<sup>13</sup> In our previous study, the beneficial effects of pitavastatin-NP were mediated by increased activity of eNOS.<sup>13</sup> Notably, NP-mediated delivery of pitavastatin had greater angiogenic activity in human endothelial cells *in vitro* compared with pitavastatin alone.<sup>13</sup> We therefore hypothesized that eNOS and downstream pathogenetic factors might be involved in the therapeutic effects of NP-mediated pitavastatin delivery on MCT-induced PAH. Among statins, pitavastatin was selected as the nanoparticulation compound because this drug elicited the most potent angiogenic effects in human endothelial cells<sup>14</sup> and the most

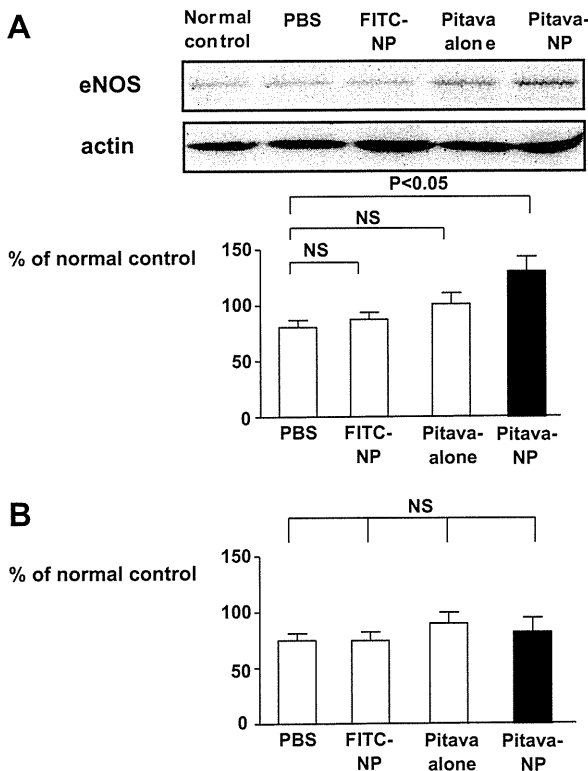


**Figure 5.** Effects of pitavastatin (pitava)-NP on eNOS protein expression. A, eNOS expression in the lung 3 days after MCT injection. The eNOS level is shown as a percentage of the internal-control actin level. n=6 per group. B, eNOS expression in the lung 21 days after MCT injection. The eNOS level is shown as a percentage of the internal-control actin level. n=6 per group.

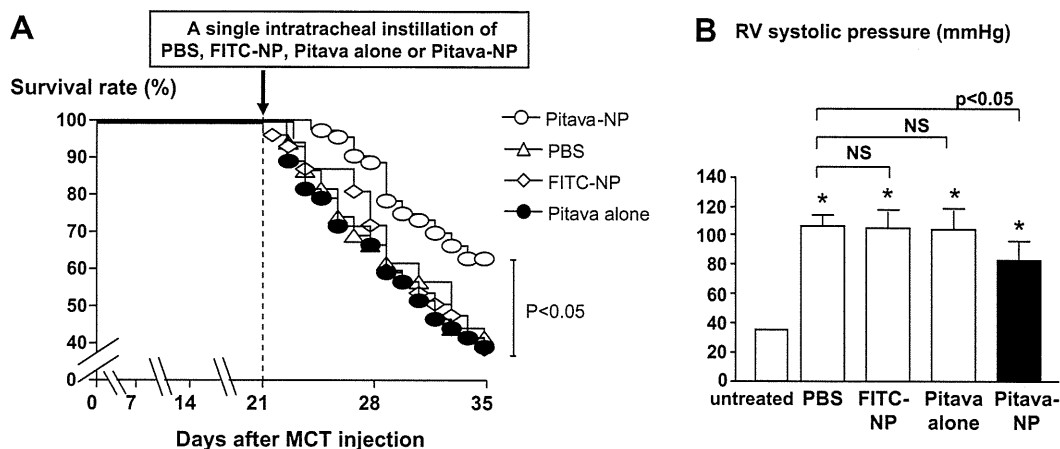


**Figure 6.** Effects of pitavastatin (pitava)-NP on RV systolic pressure and survival rate. A, Survival curves analyzed by the Kaplan-Meier method in PBS, FITC-NP, pitavastatin only, and pitavastatin-NP groups. B, RV systolic pressure (in mm Hg) in the 4 experimental groups 2 weeks after treatment (at week 5 after MCT injection).

potent inhibitory effects on human PASMC proliferation (Figure 2) in vitro compared with other statins. We also found that NP-mediated intracellular delivery of pitavastatin showed greater inhibitory effects on PASMC proliferation and on NF- $\kappa$ B activation in a monocyte cell line (RAW 264.7 cells) compared with pitavastatin alone (online-only Figures III and IV). Collectively, these in vitro data suggest that NP-mediated pitavastatin delivery is more effective than pitavastatin in inhibiting PASMC proliferation and monocyte activation and improving the deleterious effects of endothelial injury/dysfunction.

The important novel finding of the present study is that a single intratracheal instillation of pitavastatin-NP attenuated the development of PAH (increased RV pressure, PA resistance, and PA remodeling) associated with reduced activity of NF- $\kappa$ B and NF- $\kappa$ B-dependent inflammatory factors (for example, monocyte chemoattractant protein-1, IL-1, tumor necrosis factor- $\alpha$ , iNOS, etc). In contrast, eNOS expression was not reduced in the PBS group but was increased by day 3 only but not by day 21 (Figure 5), suggesting that eNOS plays a minor role in the therapeutic effects of pitavastatin-NP. Intratracheal instillation of pitavastatin alone at the same dose had no therapeutic effect. Concentrations of pitavastatin in the lungs and systemic blood were found to be similar between animals treated with pitavastatin-NP and those treated with pitavastatin only (the Table). These findings suggest a specific advantage of NP-mediated delivery of pitavastatin to induce therapeutic effects. Therefore, the beneficial effects of pitavastatin-NP on MCT-induced PAH in vivo can be attributable to the pleiotropic effects of pitavastatin-NP, including inhibition of inflammation and cell proliferation.

Prior studies have reported that daily oral administration of statins at high doses beyond the clinical norm (a regimen that could lead to serious adverse side effects in a clinical setting) attenuates MCT- and hypoxia-induced PAH in animals.<sup>7-9</sup> We thus examined whether NP-mediated pitavastatin delivery would be superior to daily oral administration of pitavastatin alone in inhibiting MCT-induced PAH, and we found that oral daily administration of pitavastatin at 0.3 mg/kg per

day for 21 days (cumulative dose=25.2 mg per animal, assuming the body weight of animals to be 250 g) had no therapeutic effects, but the same regimen of pitavastatin at 1, 3, and 10 mg/kg per day (cumulative doses=84, 252, and 840 mg per animal, respectively) did show significant therapeutic effects. Therefore, our NP-mediated delivery system (single injection of 0.1 mg pitavastatin per animal) seems to be as effective at an  $\approx$ 840-times lower dose than the cumulative systemic dose.

It is noteworthy that a single intratracheal treatment with pitavastatin-NP 3 weeks after MCT injection induced regression of PAH and improved survival rate. This finding is more clinically significant than is the mere prevention of PAH. These results suggest that this NP-mediated delivery of pitavastatin may have beneficial therapeutic effects in patients with established PAH.

### Perspectives

This mode of NP-mediated delivery of pitavastatin into the lungs is more effective in attenuating the development of MCT-induced PAH compared with intratracheal treatment with pitavastatin alone or systemic administration of pitavastatin, and treatment with pitavastatin-NP induced regression of established PAH. For translation of our present findings into clinical medicine, more clinical studies are needed to investigate whether pitavastatin-NP by inhalation might be effective in improving PAH.

### Source of Funding

This study was supported by Health Science Research grants (Research on Nano-medicine and on Intractable Diseases) from the Ministry of Health Labor and Welfare, Tokyo, Japan.

### Disclosures

Dr Egashira holds a patent on the results reported in this study. The remaining authors report no conflicts of interest.

### References

- Farber HW, Loscalzo J. Pulmonary arterial hypertension. *N Engl J Med.* 2004;351:1655-1665.
- Humbert M, Sitbon O, Simonneau G. Treatment of pulmonary arterial hypertension. *N Engl J Med.* 2004;351:1425-1436.

3. Takemoto M, Liao JK. Pleiotropic effects of 3-hydroxy-3-methylglutaryl coenzyme A reductase inhibitors. *Arterioscler Thromb Vasc Biol.* 2001; 21:1712–1719.
4. Egashira K, Hirooka Y, Kai H, Sugimachi M, Suzuki S, Inou T, Takeshita A. Reduction in serum cholesterol with pravastatin improves endothelium-dependent coronary vasomotion in patients with hypercholesterolemia. *Circulation.* 1994;89:2519–2524.
5. Egashira K. Clinical importance of endothelial function in arteriosclerosis and ischemic heart disease. *Circ J.* 2002;66:529–533.
6. Ni W, Egashira K, Kataoka C, Kitamoto S, Koyanagi M, Inoue S, Takeshita A. Anti-inflammatory and antiarteriosclerotic actions of HMG-CoA reductase inhibitors in a rat model of chronic inhibition of nitric oxide synthesis. *Circ Res.* 2001;89:415–421.
7. Girgis RE, Mozammel S, Champion HC, Li D, Peng X, Shimoda L, Tuder RM, Johns RA, Hassoun PM. Regression of chronic hypoxic pulmonary hypertension by simvastatin. *Am J Physiol.* 2007;292: L1105–L1110.
8. Nishimura T, Faul JL, Berry GJ, Vaszar LT, Qiu D, Pearl RG, Kao PN. Simvastatin attenuates smooth muscle neointimal proliferation and pulmonary hypertension in rats. *Am J Respir Crit Care Med.* 2002;166: 1403–1408.
9. Nishimura T, Vaszar LT, Faul JL, Zhao G, Berry GJ, Shi L, Qiu D, Benson G, Pearl RG, Kao PN. Simvastatin rescues rats from fatal pulmonary hypertension by inducing apoptosis of neointimal smooth muscle cells. *Circulation.* 2003;108:1640–1645.
10. McMurtry MS, Bonnet S, Michelakis ED, Bonnet S, Haromy A, Archer SL. Statin therapy, alone or with rapamycin, does not reverse monocrotaline pulmonary arterial hypertension: the rapamycin-atorvastatin-simvastatin study. *Am J Physiol.* 2007;293:L933–L940.
11. Rhodes CJ, Davidson A, Gibbs JS, Wharton J, Wilkins MR. Therapeutic targets in pulmonary arterial hypertension. *Pharmacol Ther.* 2009;121: 69–88.
12. Kimura S, Egashira K, Chen L, Nakano K, Iwata E, Miyagawa M, Tsujimoto H, Hara K, Morishita R, Sueishi K, Tominaga R, Sunagawa K. Nanoparticle-mediated delivery of nuclear factor- $\kappa$ B decoy into lungs ameliorates monocrotaline-induced pulmonary arterial hypertension. *Hypertension.* 2009;53:877–883.
13. Kubo M, Egashira K, Inoue T, Koga J, Oda S, Chen L, Nakano K, Matoba T, Kawashima Y, Hara K, Tsujimoto H, Sueishi K, Tominaga R, Sunagawa K. Therapeutic neovascularization by nanotechnology-mediated cell-selective delivery of pitavastatin into the vascular endothelium. *Arterioscler Thromb Vasc Biol.* 2009;29:796–801.
14. Oda S, Nagahama R, Nakano K, Matoba T, Kubo M, Sunagawa K, Tominaga R, Egashira K. Nanoparticle-mediated endothelial cell-selective delivery of pitavastatin induces functional collateral arteries (therapeutic arteriogenesis) in a rabbit model of chronic hind limb ischemia. *J Vasc Surg.* 2010;52:412–420.
15. Kawashima Y, Yamamoto H, Takeuchi H, Hino T, Niwa T. Properties of a peptide containing DL-lactide/glycolide copolymer nanospheres prepared by novel emulsion solvent diffusion methods. *Eur J Pharm Biopharm.* 1998;45:41–48.
16. Kawashima Y, Yamamoto H, Takeuchi H, Fujioka S, Hino T. Pulmonary delivery of insulin with nebulized DL-lactide/glycolide copolymer (PLGA) nanospheres to prolong hypoglycemic effect. *J Control Release.* 1999;62:279–287.
17. Ikeda Y, Yonemitsu Y, Kataoka C, Kitamoto S, Yamaoka T, Nishida K, Takeshita A, Egashira K, Sueishi K. Anti-monocyte chemoattractant protein-1 gene therapy attenuates pulmonary hypertension in rats. *Am J Physiol Heart Circ Physiol.* 2002;283:H2021–H2028.
18. Urboniene D, Haber I, Fang YH, Thenappan T, Archer SL. Validation of high-resolution echocardiography and magnetic resonance imaging versus high-fidelity catheterization in experimental pulmonary hypertension. *A J Physiol.* 2010;299:401–412.
19. Ohtani K, Egashira K, Nakano K, Zhao G, Funakoshi K, Ihara Y, Kimura S, Tominaga R, Morishita R, Sunagawa K. Stent-based local delivery of nuclear factor- $\kappa$ B decoy attenuates in-stent restenosis in hypercholesterolemic rabbits. *Circulation.* 2006;114:2773–2779.
20. Kojima J, Fujino H, Yosimura M, Morikawa H, Kimata H. Simultaneous determination of NK-104 and its lactone in biological samples by column-switching high-performance liquid chromatography with ultraviolet detection. *J Chromatogr.* 1999;724:173–180.
21. Hampl V, Bibova J, Banasova A, Uhlik J, Mikova D, Hnilickova O, Lachmanova V, Herget J. Pulmonary vascular iNOS induction participates in the onset of chronic hypoxic pulmonary hypertension. *Am J Physiol.* 2006;290:L11–L20.

**ONLINE SUPPLEMENT**  
**Nanoparticle-Mediated Delivery of Pitavastatin into Lungs Ameliorates  
Development and Induces Regression of Monocrotaline-induced Pulmonary  
Arterial Hypertension**

Ling Chen, Kaku Nakano, Satoshi Kimura, Tetsuya Matoba, Eiko Iwata, Miho Miyagawa, Hiroyuki Tsujimoto, Kazuhiro Nagaoka, Junji Kishimoto, Kenji Sunagawa, Kensuke Egashira

Department of Cardiovascular Medicine (LC, KN, TM, EI, MM, KN, KS, KE) and Digital Medicine Initiative (JK), Graduate School of Medical Science, Kyushu University, Fukuoka, Japan; and Hosokawa Micron Corporation (HT), Osaka, Japan.

Address for correspondence:

Kensuke Egashira, M.D. Ph.D.  
Department of Cardiovascular Medicine  
Graduate School of Medical Science, Kyushu University  
3-1-1, Maidashi, Higashi-ku,  
Fukuoka 812-8582, Japan  
Phone : +81-92-642-5358  
Fax : +81-92-642-5375  
E-mail: [egashira@cardiol.med.kyushu-u.ac.jp](mailto:egashira@cardiol.med.kyushu-u.ac.jp)

## Materials and Methods

### Echocardiographic measurements of RV and PA hemodynamics

Transthoracic 2-D, M-mode and pulsed-wave Doppler Echo were obtained with a 30 MHz transducer (Vevo 2100 ultrasound system; Primetech Inc).<sup>1</sup> M-mode and 2-D modalities were applied to measure RV free wall thickness during end diastole and RV wall stress. These images were obtained from the right side of the rat, with the ultrasonic beam positioned perpendicularly to the wall of the midthird of the RV. PA diameter was measured at the level of pulmonary outflow tract during midsystole using the superior angulation of the parasternal short-axis view. M-mode measurements were performed from “leading edge to leading edge” (epicardial to endocardial) as recommended by the American Society of Echocardiography.

Pulsed-wave Doppler was used to measure PA acceleration time (PAAT) and PA flow velocity time integral. The Doppler sample volume was centrally positioned within the main PA, just distal from the pulmonary valve with the beam oriented parallel to the flow. The sweep speed for the Doppler flow recordings was 400–800 mm/s. RV ejection time was measured as the interval from the onset to the end of ejection in milliseconds. Thereafter, pulmonary artery acceleration time normalized for cycle length, RV systolic pressure, and pulmonary vascular resistance (PVR) were estimated. Stroke volume (SV), CO, and cardiac index (CI) were also calculated.

**Measurement of lactate dehydrogenase** To examine cytotoxicity of intratracheal treatment of pitavastatin-NP, the activity of lactate dehydrogenase (LDH) in bronchoalveolar lavage fluid (BALF) and lung tissue homogenates was measured 7 days after MCT administration using an assay kit LDH (Wako Pure Chemical Industries, Ltd.) according to the manufacturer's instructions in separate series of experiments.

**Measurement of biomarkers by multiplex immunoassay** Tissue concentrations of various biomarkers in lung tissue homogenates were measured 7 days after MCT administration using the Luminex LabMAP instruments (Table III), which was ordered to biomarker analysis services of Charles River Inc (<http://www.criver.com/en-US/ProdServ/ByType/Discovery/Pages/PlasmaBiomarkerAnalysis.aspx>).

1. Urboniene D, Haber I, Fang YH, Thenappan T, Archer SL. Validation of High-Resolution Echocardiography and Magnetic Resonance Imaging Versus High-Fidelity Catheterization in Experimental Pulmonary Hypertension. *Am J Physiol Lung Cell Mol Physiol*.

Table S1. Echocardiographic characteristics of untreated control and MCT-induced PAH rats in prevention study

parameters	untreated control	MCT-induced PAH			
		PBS	FITC NP	Pitava alone	Pitava-NP
Cardiac output (mL/min)	120 ± 17	97 ± 21	104 ± 20	102 ± 20	113 ± 16
Stroke volume (mL)	0.29±0.04	0.24±0.05	0.26±0.06	0.26±0.05	0.28±0.05
Heart rate (beats per minute)	412 ± 26	408 ± 36	399 ± 39	397 ± 32	405 ± 25
PAAT/cl (x 100)	18 ± 1	7 ± 1*	7 ± 1*	7 ± 1*	12 ± 1*†
eRVSP (mmHg)	20 ± 3	65 ± 11*	66 ± 9*	62 ± 7*	41 ± 5 *†
PVR (mmHg/ml/min)	0.12 ± 0.02	0.46 ± 0.20*	0.43 ± 0.12*	0.40 ± 0.01*	0.24 ± 0.05*†
RV wall thickness (mm)	0.64 ± 0.05*	1.16 ± 0.14*	1.05 ± 0.10*	0.97 ± 0.06*	0.88 ± 0.09*†
RV wall stress	20 ± 5	48 ± 19*	56 ± 26*	48 ± 12*	24 ± 8†

Data are the mean ± SEM (n=6 each).

\*P < 0.05 versus untreated control group

† P < 0.05 versus PBS group.

Abbreviations: PAAT/cl = normalized pulmonary artery acceleration time; eRVSP = estimated RV systolic pressure; PVR = pulmonary vascular resistance.



Table S2. Lactate dehydrogenase activity in cell-free bronchial lavage fluid and lung tissue homogenates 7 days after monocrotaline administration

Sample sites	Untreated control	monocrotaline			
		PBS group	FITC NP group	Pitava alone group	Pitava NP group
bronchial lavage fluid (IU/mL)	ND	ND	ND	ND	ND
Lung tissue (IU/ng protein)	8.6±3.4	2.8±1.1	10.9±6.0	5.7±4.6	11.8±4.9

Data are the mean± SEM (n=6 each). ND = not detected (under limit of detection). There is no significant difference (P=0.56) among 5 groups by one-way ANOVA.

Table S3. Cytokines and other proteins in lung tissue homogenates 7 days after monocrotaline administration

parameters	unit	Untreated control	PBS group	FITC NP group	Pitava alone group	Pitava NP group
<b>Apo A1</b>	µg/mg	0.14±0.05	0.10±0.03	0.09±0.01	0.10±0.01	0.10±0.01
<b>CD40</b>	pg/mg	N.D.	N.D.	N.D.	N.D.	N.D.
<b>CD40 Ligand</b>	pg/mg	43±16	34±14	25±3	30±8	39±13
<b>CRP</b>	µg/mg	1.3±0.3	1.2±0.2	1.3±0.4	1.3±0.2	1.6±0.2
<b>ET-1</b>	pg/mg	61±36	67±29	61±18	64±15	56±15
<b>Eotaxin</b>	pg/mg	49±12	53±15	40±8	45±17	63±11
<b>EGF mouse</b>	pg/mg	0.54±0.21	0.55±0.21	0.40±0.08	0.44±0.09	0.44±0.07
<b>Factor VII</b>	ng/mg	0.53±0.12	0.58±0.17	0.47±0.07	0.48±0.07	0.53±0.08
<b>FGF-9</b>	ng/mg	0.10±0.02	0.09±0.03	0.07±0.01	0.08±0.01	0.08±0.03
<b>FGF-basic</b>	ng/mg	0.21±0.04	0.21±0.06	0.17±0.04	0.22±0.04	0.24±0.04
<b>GCP-2 Rat</b>	pg/mg	6.5±1.6	7.4±3.2	6.7±1.3	8.1±1.0	7.6±7
<b>GM-CSF</b>	pg/mg	N.D.	N.D.	N.D.	N.D.	N.D.
<b>Haptoglobin</b>	µg/mg	0.80±0.30	1.13±0.40	1.04±0.26	1.19±0.12	1.18±0.25
<b>IFN-gamma</b>	pg/mg	0.12±0.06	0.24±0.09	0.23±0.10	0.18±0.07	0.18±0.05
<b>IP-10</b>	pg/mg	1.7±0.3	2.2±1.0	1.7±0.3	1.7±0.5	2.1±0.8
<b>IL-1 alpha</b>	pg/mg	5.3±4.8	9.7±7.1	4.6±1.0	7.8±2.9	5.7±3.3
<b>IL-1 beta</b>	ng/mg	N.D.	N.D.	N.D.	N.D.	N.D.
<b>IL-10</b>	pg/mg	3.1±1.5	2.5±1.5	1.4±0.8	1.8±0.3	1.9±0.9
<b>IL-11</b>	pg/mg	9.8±5.6	6.1±1.6	6.1±4.8	5.9±1.0	6.8±2.0
<b>IL-12p70</b>	pg/mg	1.5±0.4	1.3±0.4	1.2±0.4	1.0±0.1	1.2±0.4
<b>IL-17A</b>	pg/mg	0.2±0.04	0.2±0.09	0.2±0.05	0.2±0.05	0.2±0.02
<b>IL-18</b>	ng/mg	0.2±0.1	0.2±0.1	0.2±0.1	0.2±0.0	0.2±0.1
<b>IL-2</b>	pg/mg	1.7±0.7	1.4±1.1	0.6±0.3	0.8±0.6	0.9±0.7
<b>IL-3</b>	pg/mg	1.1±0.5	0.9±0.3	0.9±0.4	0.7±0.3	0.8±0.2
<b>IL-4</b>	pg/mg	N.D.	N.D.	N.D.	N.D.	N.D.
<b>IL-5</b>	ng/mg	N.D.	N.D.	N.D.	N.D.	N.D.
<b>IL-6</b>	pg/mg	N.D.	N.D.	N.D.	N.D.	N.D.
<b>IL-7</b>	pg/mg	3.9±0.7	3.5±2.0	3.4±0.8	3.0±0.3	3.2±0.6
<b>LIF</b>	pg/mg	33.9±9.8	38.3±12.5	29.9±4.3	31.6±4.1	35.7±6.1
<b>Lymphotactin</b>	pg/mg	1.7±0.4	2.0±0.7	1.8±0.3	1.6±0.1	1.78±0.4
<b>MIP-1alpha</b>	ng/mg	0.05±0.02	0.06±0.02	0.05±0.01	0.05±0.00	0.05±0.01
<b>MIP-1beta</b>	pg/mg	26.7±7.6	36.8±13.2	30.9±13.2	27.1±5.2	28.2±5.8
<b>MIP-2</b>	pg/mg	1.7±1.0	1.3±0.3	1.5±0.5	1.8±0.9	1.8±0.5
<b>MIP-3 beta</b>	ng/mg	0.1±0.0	0.2±0.1	0.1±0.0	0.2±0.0	0.2±0.0
<b>MDC</b>	pg/mg	14±5	11±3	12±1	15±5	15±3
<b>MMP-9</b>	pg/mg	16±3	13±6	13±3	14±3	13±3
<b>MCP-1</b>	pg/mg	14±2	17±4	17±4	16±4	20±4
<b>MCP-3</b>	pg/mg	12±3	14±4	13±3	13±3	16±4
<b>MPO</b>	ng/mg	26±12	25±14	15±4	15±5	26±6
<b>Myoglobin</b>	ng/mg	109±26	157±130	138±67	135±54	133±69
<b>OSM</b>	pg/mg	9±2	11±3	9±1	9±0.001	10±2
<b>SAP</b>	pg/mg	0.007±0.002	0.007±0.002	0.006±0.001	0.008±0.001	0.008±0.001
<b>SGOT</b>	µg/mg	N.D.	N.D.	N.D.	N.D.	N.D.
<b>SCF</b>	pg/mg	920±509	404±71	421±143	603±440	531±110
<b>RANTES</b>	pg/mg	0.82±0.51	0.55±0.35	0.56±0.50	0.56±0.31	0.56±0.25
<b>TPO</b>	ng/mg	0.41±0.09	0.39±0.15	0.32±0.11	0.23±0.14	0.27±0.08
<b>TF</b>	ng/mg	0.15±0.03	0.15±0.05	0.15±0.03	0.14±0.03	0.14±0.04

<b>TIMP-1</b>	pg/mg	4±8	3.8±1.2	3.6±0.8	3.5±0.5	3.6±0.6
<b>TNF-alpha</b>	ng/mg	2.4±0.5	2.7±0.7	2.3±0.5	2.1±0.2	2.2±0.5
<b>VCAM-1</b>	ng/mg	4.8±1.0	5.4±1.8	5.2±1.0	5.2±0.9	5.8±0.7
<b>VEGF-A</b>	pg/mg	749±297	759±281	924±317	791±181	689±214
<b>vWF</b>	ng/mg	0.6±0.2	0.5±0.2	0.4±0.1	0.5±0.1	0.5±0.1

Data are mean ± SEM (n= 6 each).

Multiplex immunoassay were performed using the Luminex LabMAP instruments.

Apo A1 (Apolipoprotein A1), CD (cluster of differentiation), CRP (C Reactive Protein), EGF (Epidermal Growth Factor), FGF-9 (Fibroblast Growth Factor-9), FGF-basic (Fibroblast Growth Factor-basic), GCP-2 (Granulocyte Chemotactic Protein-2), GM-CSF (Granulocyte Macrophage-Colony Stimulating Factor), GST-a (Glutathione S-Transferase alpha), IFN-g (Interferon-gamma), IgA (Immunoglobulin A), IL (Interleukin), IP-10 (Inducible Protein-10), LIF (Leukemia Inhibitory Factor), MCP (Monocyte Chemoattractant Protein), MDC (Macrophage-Derived Chemokine), MIP (Macrophage Inflammatory Protein), MMP-9 (Matrix Metalloproteinase-9), MPO (Myeloperoxidase), OSM (Oncostatin M), RANTES (Regulation Upon Activation, Normal T-Cell Expressed and Secreted), SAP (Serum Amyloid P), SCF (Stem Cell Factor), SGOT (Serum Glutamic-Oxaloacetic Transaminase), TIMP-1 (Tissue Inhibitor of Metalloproteinase Type-1), TNF-a (Tumor Necrosis Factor-alpha), TPO (Thrombopoietin), VCAM-1 (Vascular Cell Adhesion Molecule-1), VEGF (Vascular Endothelial Cell Growth Factor), vWF (von Willebrand Factor). N.D. (Not Detected).

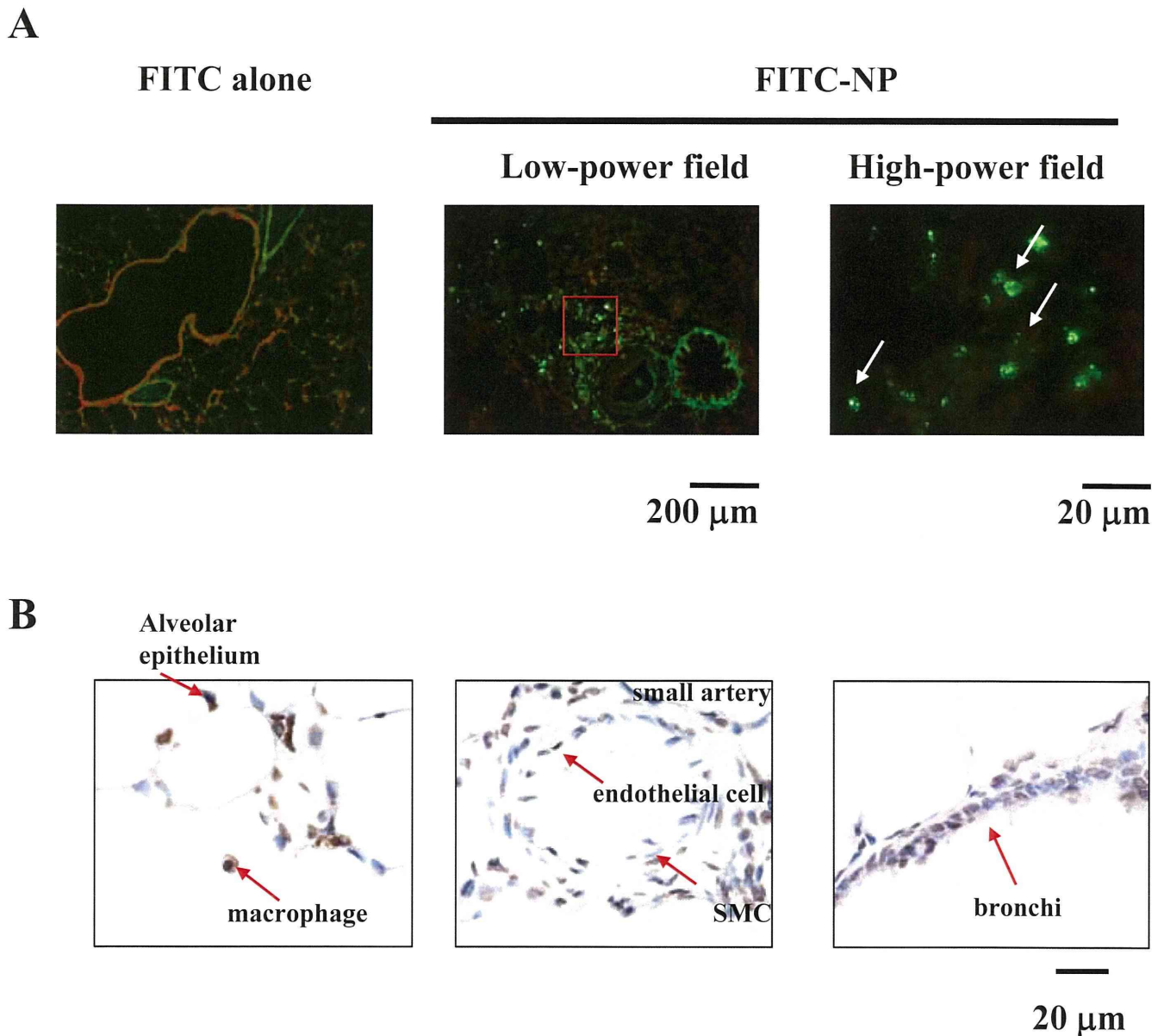


**Figure S1.** Localization of FITC alone and FITC-NP post-instillation in the rat lung. A, Fluorescent micrographs of cross-sections from lung instilled with FITC alone and FITC-labeled NP on day 3 post-instillation. Nuclei were counterstained with propidium iodide (red). Scale bars: 200  $\mu\text{m}$  and 20  $\mu\text{m}$ . B, Micrographs of cross-sections stained immunohistochemically against FITC from lung instilled intratracheally with FITC-NP on days 14 post-instillation.